Healthcare Analytics 4 (2023) 100240

Contents lists available at ScienceDirect

Healthcare Analytics

journal homepage: www.elsevier.com/locate/health

A non-linear differential equation model of COVID-19 and seasonal influenza co-infection dynamics under vaccination strategy and immunity waning

Rabiu Musa [a], Olumuyiwa James Peter [b,c,*], Festus Abiodun Oguntolu [d]

[a] Faculty of Mathematics, Technion Israel Institute of Technology, Haifa 32000, Israel
[b] Department of Mathematical and Computer Sciences, University of Medical Sciences, Ondo City, Ondo State, Nigeria
[c] Department of Epidemiology and Biostatistics, School of Public Health, University of Medical Sciences, Ondo City, Ondo State, Nigeria
[d] Department of Mathematics, Federal University of Technology, Minna, Niger State, Nigeria

ARTICLE INFO

Keywords:
Non-linear differential equation
Co-infection
Seasonal influenza
COVID-19
Vaccination
Immunity waning

ABSTRACT

This study presents a mathematical model of the transmission dynamics of COVID-19 and influenza co-infection. The potential impacts of the influenza vaccine only on the co-infection dynamics and the potential impacts of both vaccines on the co-infection dynamics are thoroughly studied. The basic reproduction number for the two diseases using the next-generation matrix approach and the stability of the sub-model is examined. The model assessed the scenario whereby both diseases' waning immunity occurs concurrently to check the epidemic peaks. The numerical simulation results show that the diseases would continue to be endemic in the population if the immunity waning rates increase. The epidemic peak can be reduced by increasing vaccination and vaccine efficacy rates. The results show that the COVID-19 contact rate significantly increases the epidemic level more than the co-infection contact rate. A similar result was obtained when it was observed that the COVID-19 post-recovery waning rate has more significant effects on the epidemic peak than the co-infection post-recovery waning rate. A possible reason for this counter-intuitive occurrence is that two infections cannot have the same viral load nor the same within-host competitiveness. This means an infectious co-infected person will transmit the infection with the highest within-host competitiveness. Here, it is suspected that COVID-19 has a within-host competitive advantage over influenza in the co-dynamics.

1. Introduction

The novel coronavirus disease 2019 (COVID-19) was discovered in December 2019 in Wuhan, China [1,2]. The new disease spreads across the globe within a short time resulting in over 6.6 million deaths and over 600 million reported cases as of November 2022 [3]. COVID-19 disease, like the common cold, severe acute respiratory syndrome (SARS), and Middle East respiratory syndrome (MERS) is caused by severe acute respiratory syndrome coronavirus 2 (SARS-CoV-2) [4] though COVID-19 is more infectious and deadlier compared to the aforementioned diseases. In March 2020, the World Health Organization (WHO) declared the COVID-19 outbreak a pandemic [4,5].

Through the inhalation of infectious aerosols released when an infected person talks, sneezes, or coughs, the virus can be spread directly from one person to another. A susceptible person may contract the virus if they come into contact with an infected person by touching, kissing, holding, and other behaviors. The hands are used to touch the eyes, nose, and mouth in the indirect transmission method, which requires touching a contaminated surface [6,7].

The public was urged to concentrate on non-pharmaceutical measures by the government and decision-makers before vaccines were introduced. These non-pharmaceutical therapies include good personal cleanliness, proper coughing technique, social distancing, closure of schools, quarantine, hospitalization of exposed and infected persons, contact tracing, and wearing of face masks [8,9]. Rapid vaccination, intensive medical care, and screening of exposed individuals were also implemented to limit the number of cases [10,11]. The disease kept evolving despite the existence of infection controls and prevention measures in numerous nations around the world. It began with alpha, progressed through beta, and delta, and it is currently continuing with the ongoing omicron variant [12,13], which greatly increases the number of infected people and the fatality rate.

The viral influenza disease usually referred to as the flu, has long been a source of concern for public health practitioners. Approximately 500,000 individuals per year lose their lives to seasonal influenza outbreaks, which afflict millions of people [14,15]. Although there is growing evidence that aerosols are important in the spread of influenza, it has been shown that only close contact with droplets and direct contact with an infected person may transfer influenza dynamics

* Corresponding author at: Department of Mathematical and Computer Sciences, University of Medical Sciences, Ondo City, Ondo State, Nigeria.
E-mail address: peterjames4real@gmail.com (O.J. Peter).

https://doi.org/10.1016/j.health.2023.100240
Received 22 April 2023; Received in revised form 27 July 2023; Accepted 28 July 2023

[16,17]. Common symptoms include muscle aching, lack of appetite, fever, cough, headaches, and sore throat. Because of how much these symptoms resemble COVID-19 symptoms, diagnosis and therapy might be challenging [14,15].

Due to the seasonality of influenza outbreaks and COVID-19's ongoing prevalence, influenza and COVID-19 could co-circulate, significantly raising the chance of co-infection. Although limited information is available on the epidemiological and clinical outcomes of co-infection, the available research has found that co-infection with the influenza virus increases COVID-19's infectivity in a wide variety of cell types [18], while co-infected patients appear to have similar clinical symptoms and radiological images compared to patients infected with COVID-19 alone [19]. The clinical presentation, transmission mechanism, and characteristics of influenza and COVID-19 are so similar that diagnosing and initiating proper treatment for the two conditions are very challenging. In the context of the COVID-19 pandemic, the co-infection of COVID-19 and influenza could place additional strain on healthcare services by consuming scarce medical resources, making treatment more challenging, and increasing prognosis uncertainty. The World Health Organization (WHO) has long advocated for annual influenza vaccination as a means of preventing the disease, particularly in high-risk groups that are more susceptible to illness such as pregnant women and older adults (aged > 55). Numerous mathematical models have been formulated since the novel coronavirus disease pandemic in 2020 in order to better understand transmission dynamics and potential management measures. Some of these studies includes [20–32] and the references therein. Seasonal influenza vaccine is thought to provide additional benefits in the challenging COVID-19 pandemic phase, in addition to serving a significant role in influenza prevention. The potential danger of respiratory infectious diseases like COVID-19 is significantly decreased as a result of influenza vaccination, which also lessens the strain on healthcare systems and frees up resources for the treatment of more serious illnesses [33]. Additionally, it is thought that receiving an influenza vaccine improves both the specificity and accuracy of COVID-19 surveillance [34]. In the literature, we discovered a link between the influenza vaccine and a decreased risk of SARS-CoV-2 infection. One hypothesis is that those who had influenza vaccine in previous seasons seemed to be more health-conscious, thus they may have adhered to COVID-19 prevention strategies such as social distancing and mask use more consistently, lowering their chance of infection. Additionally, getting vaccinated against influenza may lower your risk of getting sick, which lowers your risk of visiting the hospital and contracting SARS-CoV-2 in high-risk settings like hospitals.

One of the challenges faced by medical practitioners in curing the spread of infectious diseases is the waning of immunity to diseases. Basically, there are two types of immunity: vaccine-induced immunity and post-recovery immunity. The immunity to infectious diseases that vaccines provide is either temporal or permanent. A rise in immune cells and antibodies that serve as the "front-line fighters" against an outside invader in the body, such as a virus, occurs days after vaccination. These "front-line combatants" inevitably dwindle or diminish over time, but they never disappear completely. All vaccines result in this, which is expected and typical. After this first reaction, the immune system is still prepared to "protect", with long-lasting "memory" B and T cells present in the body that are prepared to create antibodies and fight the disease they later encounter [35,36].

A few researchers have studied the co-infection dynamics of COVID-19 and Influenza virus [17,37] other available works are clinical studies [38–40] and systematic review [41,42]. The co-infection of COVID-19 and Influenza virus was studied by [37] using two mathematical models of COVID-19 and co-infection model (SARS-CoV-2 and influenza virus) using SimBiology toolbox from Matlab v7.11.1.866. Understanding signaling regulation in COVID-19 and co-infection model systems aid in the development of network-based models thereby suggesting intervention points for therapeutics. The study shows the aim of revealing such perturbations to decipher opportune mediating cross-talks characterizing the virus. The comparative analysis of both the models reveals major signaling protein NFjB and STAT1 which is responsible for co-infection. Their results show that the co-infection of both viruses results in higher production of inflammatory proteins indicating that the co-infection state is more dangerous than the COVID-19 or influenza state alone. They further suggest that this condition can be brought under control if the production of these inflammatory proteins is regulated at the cellular level.

Using 15 systems of ordinary differential equations and optimal control theory, [17] studied the co-infection dynamics of COVID-19 and influenza virus using an endemic model. Their model shows the stability of the equilibria (disease-free and endemic) depending on the value of the reproduction number. Their results show that disease competitive dynamics in the population are determined by transmission probabilities and threshold quantities. After analyzing the optimal control problem incorporated into the model, their analyses show that, though single and two-fold control interventions can be used to reduce the disease burden, the simultaneous implementation of all three control strategies will be the most effective way to eliminate COVID-19 and influenza in the population.

The study carried out by [38] reported 6 cases of co-infection of COVID-19 and influenza. All patients with COVID-19 diagnoses were included. All patients with a suspected COVID-19 diagnosis underwent standard influenza screenings. The radiography of their thorax was examined for COVID-19 and influenza. 1103 patients with COVID-19 were diagnosed during the study period. Six of them (or 0.54%) were found to have influenza and other infections with 28 co-infected cases. Findings from thorax radiography were consistent with COVID-19 in five patients and influenza in one. Their condition ranged in intensity from mild to moderate. Patients who died ($n = 2$) as well as those who were ventilator-dependent or receiving mechanical ventilation were among the cases that were documented in the literature.

The researchers in [41] did a systematic review and metadata analysis of COVID-19 and influenza co-infection. The findings show that patients with COVID-19 and co-infection rate with the influenza virus was 4.5% in Asia and 0.4% in America. There were 30 men and 31 women among the patients in four prevalence studies. Co-infection with influenza was present in 5.3 and 9.1 percent of men and women with COVID-19, respectively. A total of 123 patients with COVID-19 were included in eight case reports and seven case series; 29 of these patients (16 men and 13 women) with a mean age of 48 years had concurrent infection with influenza viruses A and B.

In this study, a new deterministic co-infection model of COVID-19 and influenza virus incorporating vaccination, vaccine-induced immunity waning, and post-recovery immunity waning is analyzed. The main idea behind the incorporation of immunity waning was that toward the middle of 2021, it was reported that vaccinated individuals are experiencing a breakthrough of infection [43–45] and waning of both natural and vaccine-induce immunity [35,36]. We believe that the incorporation of this phenomenon and its impacts on the co-dynamics of both diseases will be of great interest not only to public health workers but also to researchers in the field of mathematical modeling. The aim of this paper is to analyze the dynamics and stability properties of the model equations and examine the effects of the COVID-19 vaccine on the prevalence of influenza and vice versa. We shall also examine the potential impacts of vaccine efficacy, transmission rates, and immunity waning on the dynamics of the viruses.

The rest of the paper is structured down as follows. The formulation of the co-infection model, description of model state variables, model assumptions, and definition of all model parameters are presented in Section 2. We analyze the COVID-19-only and the influenza-only model in Sections 3.1 and 3.2 respectively. The analyses include non-negativity and boundedness of solutions, reproduction number, and stability properties of the disease-free and endemic equilibria. The co-infection-free equilibrium and the reproduction number complete the section. In Section 4, numerical simulations of the ODE system for hypothetical scenarios such as the potential effects of the vaccination and immunity waning are presented. Lastly, modeling results are extensively discussed in Section 5.

2. Mathematical model

The co-infection of COVID-19 with other respiratory pathogens, which could impede COVID-19 diagnosis, treatment, and prognosis, has recently come to light as a source of concern. These concomitant infections could even worsen illness symptoms and mortality [41,46]. Wide administration of vaccines has been one of the most effective preventive measures but the loss of vaccine-induced immunity and waning of post-recovery has been a big impediment in curbing the epidemic. A 12-compartmental co-infection model of COVID-19 and seasonal influenza is formulated and analyzed. The co-dynamics population at any time t is represented by $N(t)$. The population is stratified into the mutually exclusive populations of susceptible $S(t)$, COVID-19 exposed class $E_c(t)$, and co-infection exposed class $E_{ci}(t)$. The vaccinated individuals against COVID-19, influenza, and both diseases are respectively denoted by $V_c(t), V_i(t)$ and $V_{ci}(t)$. The COVID-19, influenza and co-infected individuals respectively denoted by $I_c(t), I_i(t)$ and I_{ci} become recovered and move to the compartments $R_c(t), R_i(t)$ and $R_{ci}(t)$ respectively.

The total population is given by

$$N = S + V_c + E_c + I_c + R_c + V_i + I_i + R_i + V_{ci} + E_{ci} + I_{ci} + R_{ci}, \quad (2.1)$$

we note here that the individuals in the exposed compartment are the newly infected individuals that are not yet infectious.

The susceptible class is populated by the recruitment rate Λ (either by migration or by birth), waning immunity rate of COVID-19, influenza, and co-infected recovered individuals $\omega_c, \omega_i, \omega_{ci}$ (ie. the post-recovery waning rate of those who recovered from COVID-19, influenza and both diseases respectively) and waning immunity rate of COVID-19, influenza and co-infected vaccinated individuals $\tau_c, \tau_i, \tau_{ci}$ (ie. the vaccine waning rate of those who are vaccinated against COVID-19, influenza and both diseases respectively). The susceptible class is depopulated by the vaccination rate θ (where $\theta = \theta_c$(COVID-19 vaccination rate) + θ_i(influenza vaccination rate) + θ_{ci} (co-infection vaccination rate)), natural death rate μ and $\lambda = \lambda_c + \lambda_i + \lambda_{ci} + \lambda_{ic}$ denoting the force of infection for the COVID-19, influenza and co-infection transmission respectively. The model equation for the susceptible class is given by

$$\frac{dS}{dt} = \Lambda + \omega_c R_c + \omega_i R_i + \omega_{ci} R_{ci} + \tau_c V_c + \tau_i V_i + \tau_{ci} V_{ci} - (\theta + \mu + \lambda)S. \quad (2.2)$$

The forces of infection are expressed as

$$\lambda_c = \frac{\beta_c I_c}{N_c}, \ \lambda_i = \frac{\beta_i I_i}{N_i}, \ \lambda_{ic} = \frac{\beta_{ic} I_{ci}}{N} \text{ and } \lambda_{ci} = \frac{\beta_{ci} I_{ci}}{N}, \quad (2.3)$$

where the parameters $\beta_c, \beta_i, \beta_{ci}$ and β_{ic} denote the effective contact rate leading to COVID-19, influenza transmission, and co-infection of both diseases. We need to mention here that susceptible individuals can be vaccinated against both diseases since there is no universal vaccine against both infections which means that immunity against one does not guarantee immunity against the other.

The COVID-19 vaccinated class is made up of the vaccination rate θ_c and decreases by the breakthrough of infection among the vaccinated individuals at the rate $(1 - \epsilon_c)\lambda V$ for all the three infection categories of COVID-19, influenza and both while the vaccine is assumed to be imperfect [47–49] with vaccine efficacy rate ϵ_c where $0 \le \epsilon_c \le 1$. The population is further decreased by natural death rate μ and vaccine-induced immunity waning rate τ_c so that the compartment is given by

$$\frac{dV_c}{dt} = \theta_c S - (1 - \epsilon_c)\lambda V_c - (\tau_c + \mu)V_c. \quad (2.4)$$

The Influenza vaccinated class is made up of the vaccination rate θ_i and decreases by the breakthrough of infection among the vaccinated individuals at the rate $(1 - \epsilon_i)\lambda V_i$ for all the three infection categories of COVID-19, influenza, and both while the vaccine is assumed to be imperfect with vaccine efficacy rate ϵ_i where $0 \le \epsilon_i \le 1$. The population is further decreased by natural death rate μ and vaccine-induced immunity waning rate τ_i so that the compartment is given by

$$\frac{dV_i}{dt} = \theta_i S - (1 - \epsilon_i)\lambda V_i - (\tau_i + \mu)V_i. \quad (2.5)$$

The class of those who are vaccinated against both diseases is made up of the vaccination rate θ_{ci} and decreases by the breakthrough of infection among the vaccinated individuals at the rate $(1 - \epsilon_{ci})\lambda_{ci} V_{ci}$ (where $0 \le \epsilon_{ci} \le 1$) while the vaccine is assumed to be imperfect with vaccine efficacy rate ϵ_{ci}. The population is further decreased by natural death rate μ and vaccine-induced immunity waning rate τ_{ci}. Hence, we have

$$\frac{dV_{ci}}{dt} = \theta_{ci} S - (1 - \epsilon_{ci})\lambda_{ci} V_{ci} - (\tau_{ci} + \mu)V_{ci}. \quad (2.6)$$

The class E_c of those who are exposed to COVID-19 is populated by the forces of infection $(\lambda_c + \lambda_{ci})$ for COVID-19 and co-infected individuals moving from the susceptible class, breakthrough of infection from COVID-19 vaccinated individuals $(1 - \epsilon_c)(\lambda_c + \lambda_{ci})V_c$ and influenza vaccinated individuals $(1 - \epsilon_i)(\lambda_c + \lambda_{ci})V_i$. The class is decreased by natural death rate μ and COVID-19 progression rate from E_c to I_c denoted by σ_c. Hence, we have

$$\frac{dE_c}{dt} = (\lambda_c + \lambda_{ci})[S + (1 - \epsilon_c)V_c] + (1 - \epsilon_i)(\lambda_c + \lambda_{ci})V_i - (\sigma_c + \mu)E_c. \quad (2.7)$$

The COVID-19 infected class is decreased by recovery rate γ_c, natural death rate μ, COVID-19 induced death rate δ_c, and $\phi_i \lambda_i$ which accounts for the assumed reduction in susceptibility to COVID-19 after being already infected with influenza. The class is given by

$$\frac{dI_c}{dt} = \sigma_c E_c - (\gamma_c + \mu + \delta_c + \phi_i \lambda_i)I_c. \quad (2.8)$$

From the above explanations, the COVID-19 recovered class is given by

$$\frac{dR_c}{dt} = \gamma_c I_c - (\omega_c + \mu)R_c. \quad (2.9)$$

The influenza-infected class I_i is populated by the forces of infection of influenza and co-infected individuals moving from the susceptible class $(\lambda_i + \lambda_{ic})S$, the breakthrough of infection from influenza-vaccinated individuals $(1 - \epsilon_i)(\lambda_i + \lambda_{ic})V_i$ and COVID-19 vaccinated individuals $(1 - \epsilon_i)(\lambda_c + \lambda_{ci})V_i$. The class is decreased by natural death rate μ, recovery rate γ_i, and influenza-induced death rate δ_i. Hence, we have

$$\frac{dI_i}{dt} = (\lambda_i + \lambda_{ic})[S + (1 - \epsilon_i)V_i] + (1 - \epsilon_c)(\lambda_i + \lambda_{ic})V_c - (\gamma_i + \delta_i + \mu)I_i. \quad (2.10)$$

From the above explanations, the class of those who recover from influenza is given by

$$\frac{dR_i}{dt} = \gamma_i I_i - (\omega_i + \mu)R_i. \quad (2.11)$$

The class E_{ci} of those who are exposed to the two diseases is made up of the force of infection of those who experienced the breakthrough of infection after being vaccinated against both diseases denoted by $(1 - \epsilon_{ci})\lambda_{ci} V_{ci}$, $\phi_i \lambda_i$ (for influenza as explained above), $\phi_c \lambda_c$ (for COVID-19 as explained above). It is being reduced by the progression rate σ_{ci} from E_{ci} to I_{ci} and the natural death rate. The class is given by

$$\frac{dE_{ci}}{dt} = (1 - \epsilon_{ci})\lambda_{ci} V_{ci} + \phi_i \lambda_i I_c + \phi_c \lambda_c I_i - (\sigma_{ci} + \mu)E_{ci}. \quad (2.12)$$

The class I_{ci} of those who are co-infected with both diseases is populated by σ_{ci} and depopulated by the recovery rate γ_{ci}, co-infection-induced death rate δ_{ci}, and natural death rate μ so that the class is given by

$$\frac{dI_{ci}}{dt} = \sigma_{ci} E_{ci} - (\gamma_{ci} + \mu + \delta_{ci})I_{ci}. \quad (2.13)$$

From all the above explanations, the class of those who recovered from both infections is given by

$$\frac{dR_{ci}}{dt} = \gamma_{ci} I_{ci} - (\omega_{ci} + \mu)R_{ci}. \quad (2.14)$$

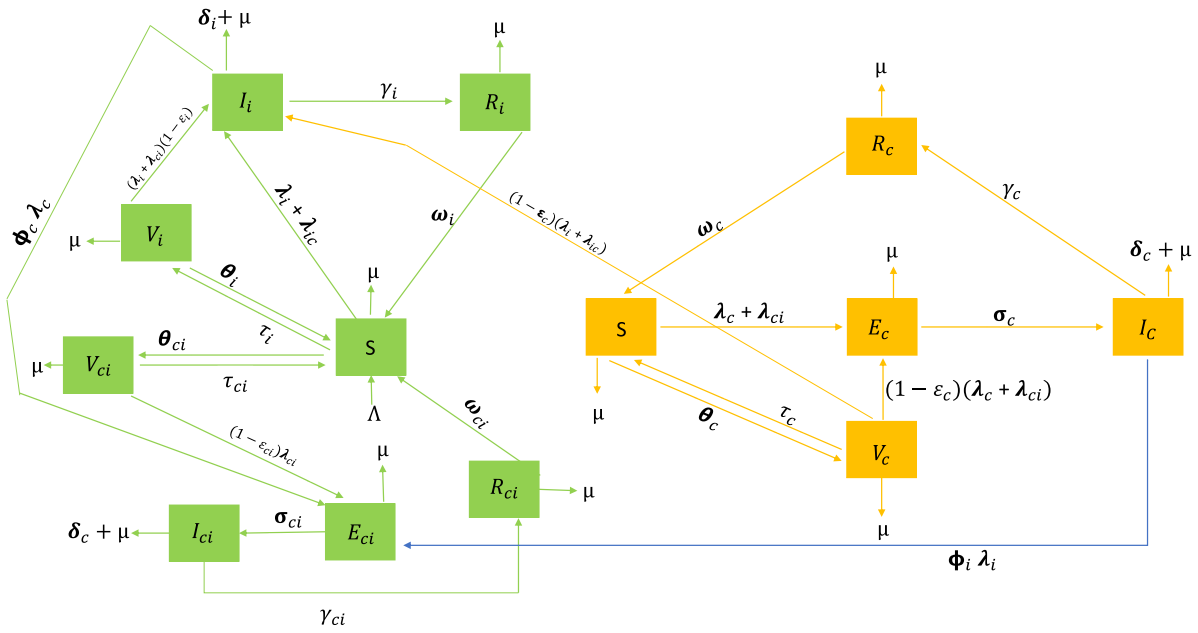

Fig. 1. The Flow-diagram. The population is stratified into the mutually exclusive populations of susceptible $S(t)$, COVID-19 exposed class $E_c(t)$, and co-infection exposed class $E_{ci}(t)$. The vaccinated individuals against COVID-19, influenza, and both diseases are respectively denoted by $V_c(t), V_i(t)$ and $V_{ci}(t)$. The COVID-19, influenza and co-infected individuals respectively denoted by $I_c(t), I_i(t)$ and I_{ci} become recovered and move to the compartments $R_c(t), R_i(t)$ and $R_{ci}(t)$ respectively.

Table 1
Model variables and descriptions.

Variable	Description
S	Susceptible population
V_c, V_i, V_{ci}	Vaccinated COVID-19, influenza and co-infected populations respectively
R_c, R_i, R_{ci}	Recovered individuals from COVID-19, influenza and co-infection respectively
I_c, I_i, I_{ci}	COVID-19, influenza and co-infected populations respectively
E_c, E_{ci}	Exposed COVID-19 and co-infected populations respectively

The model equation for the total population is given by

$$
\begin{aligned}
\frac{dS}{dt} &= \Lambda + \omega_c R_c + \omega_i R_i + \omega_{ci} R_{ci} + \tau_c V_c + \tau_i V_i + \tau_{ci} V_{ci} - (\theta + \mu + \lambda)S,\\
\frac{dV_c}{dt} &= \theta_c S - (1-\epsilon_c)\lambda V_c - (\tau_c + \mu)V_c,\\
\frac{dE_c}{dt} &= (\lambda_c + \lambda_{ci})[S + (1-\epsilon_c)V_c] + (1-\epsilon_i)(\lambda_c + \lambda_{ci})V_i - (\sigma_c + \mu)E_c,\\
\frac{dI_c}{dt} &= \sigma_c E_c - (\gamma_c + \mu + \delta_c + \phi_i\lambda_i)I_c,\\
\frac{dR_c}{dt} &= \gamma_c I_c - (\omega_c + \mu)R_c\\
\frac{dV_i}{dt} &= \theta_i S - (1-\epsilon_i)\lambda V_i - (\tau_i + \mu)V_i,\\
\frac{dI_i}{dt} &= (\lambda_i + \lambda_{ic})[S + (1-\epsilon_i)V_i] + (1-\epsilon_c)(\lambda_i + \lambda_{ic})V_c\\
&\quad - (\gamma_i + \delta_i + \mu + \phi_c\lambda_c)I_i,\\
\frac{dR_i}{dt} &= \gamma_i I_i - (\omega_i + \mu)R_i,\\
\frac{dV_{ci}}{dt} &= \theta_{ci} S - (1-\epsilon_{ci})\lambda_{ci} V_{ci} - (\tau_{ci} + \mu)V_{ci},\\
\frac{dE_{ci}}{dt} &= (1-\epsilon_{ci})\lambda_{ci} V_{ci} + \phi_i\lambda_i I_c + \phi_c\lambda_c I_i - (\sigma_{ci} + \mu)E_{ci},\\
\frac{dI_{ci}}{dt} &= \sigma_{ci} E_{ci} - (\gamma_{ci} + \mu + \delta_c)I_{ci},\\
\frac{dR_{ci}}{dt} &= \gamma_{ci} I_{ci} - (\omega_{ci} + \mu)R_{ci}
\end{aligned}
\tag{2.15}
$$

with the following initial conditions

$$
\begin{aligned}
&S(0) > 0, V_c \geq 0, E_c \geq 0, I_c \geq 0, R_c \geq 0, V_i \geq 0, I_i \geq 0, R_i \geq 0,\\
&V_{ci} \geq 0, E_{ci} \geq 0, I_{ci} \geq 0, \text{ and } R_{ci} \geq 0.
\end{aligned}
\tag{2.16}
$$

Another assumption of the model is that since two infections cannot have the same viral load nor can they have the same within-host competitiveness, this means that an infectious co-infected person will transmit the infection that has the highest within-host competitiveness. Therefore, λ_{ci} is the force of infection that indicates when COVID-19 has the within-host competitive advantage over influenza, while λ_{ic} is the force of infection that indicates when influenza has the within-host competitive advantage over COVID-19. The parameter β_{ci} indicates that COVID-19 is transmitted in infectious co-infected individuals, while β_{ic} indicates that influenza is transmitted in infectious co-infected individuals. Consequently, if COVID-19 has the highest competitive advantage over influenza, then $\delta_{ci} = \delta_c$, and if it is the other way round, then $\delta_{ic} = \delta_i$. It is also worth noting that the order of infection does not matter in the stratification of the co-dynamics population classes i.e $E_{ci} = E_{ic}, V_{ci} = V_{ic}, I_{ci} = I_{ic}, R_{ci} = R_{ic}$ that is why the reverse-order of the co-dynamics classes are ignored (see Fig. 1).

The model variables and their descriptions are given in Table 1.

The model parameters and descriptions are given in Table 2.

3. Model analysis

In this section, we shall analyze the COVID-19 sub-model qualitatively. These analyses include the boundedness of the solution, positivity of the solution, the existence of disease-free and endemic equilibria,

Table 2
Model parameters, descriptions, and values.

Parameter	Description	Value	Reference
Λ	Birth and immigration rate	52,272/year	Estimated from [50,51]
β_c	Effective contact rate leading to COVID-19	0.5249	[17,52]
β_i	Effective contact rate leading to influenza	0.2530	[53]
β_{ci}, β_{ic}	Effective contact rate leading to co-infection	0.4320, 0.4320	Assumed
τ_c	Waning rate of COVID-19 vaccine	$0 \le \tau_c \le 1$	
τ_i	Waning rate of influenza vaccine	$0 \le \tau_i \le 1$	
τ_{ci}	Waning rate of both vaccines	$0 \le \tau_{ci} \le 1$	
ω_c	Post-recovery waning rate after COVID-19 infection	$0 \le \omega_c \le 1$	
ω_i	Post-recovery waning rate after influenza infection	$0 \le \omega_i \le 1$	
ω_{ci}	Post-recovery waning rate after co-infection	$0 \le \omega_{ci} \le 1$	
δ_c	COVID-19-induced death rate	0.0014	[54,55]
δ_i	Influenza-induced death rate	0.0210	[56]
θ_c	COVID-19 vaccination rate	$0 \le \theta_c \le 1$	
θ_i	Influenza vaccination rate	$0 \le \theta_i \le 1$	
θ_{ci}	Vaccination rate of those who take both vaccines	$0 \le \theta_{ci} \le 1$	
ϵ_c	Efficacy of COVID-19 vaccine	$0 \le \epsilon_c \le 1$	
ϵ_i	Efficacy of influenza vaccine	$0 \le \epsilon_i \le 1$	
ϵ_{ci}	Efficacy of both vaccines	$0 \le \epsilon_{ci} \le 1$	
σ_c	Progression rate from E_c to I_c	1/2 day^{-1}	[57,58]
σ_{ci}	Progression rate from E_{ci} to I_{ci}	1/5 day^{-1}	Assumed
ϕ_c	Assumed susceptibility to COVID-19 after influenza infection	0.225	Assumed
ϕ_i	Assumed susceptibility to influenza after COVID-19 infection	0.3225	Assumed
μ	Natural death rate	0.0121	[59]
γ_c	Recovery rate after COVID-19 infection	1/7 day^{-1}	[54,60]
γ_i	Recovery rate after influenza infection	0.1998	[56]
γ_{ci}	Recovery rate after co-infection	0.1880	Assumed

and the threshold quantities. We shall also examine the possibility of backward bifurcation. Lastly, we shall establish the same analyses for the influenza sub-model.

3.1. Analysis of the COVID-19 sub-model

For the COVID-19 sub-model, we shall set all influenza and co-infection-related parameters and variables to zero. These variables are $V_i = V_{ci} = R_i = R_{ci} = I_i = I_{ci} = E_i = E_{ci} = 0$ and the parameters include $\beta_i = \beta_{ci} = \tau_i = \tau_{ci} = \omega_i = \omega_{ci} = \delta_i = \delta_{ci} = 0$ among others. The COVID-19 sub-model is given by

$$\begin{aligned}
\frac{\mathrm{d}S_c}{\mathrm{d}t} &= \Lambda + \omega_c R_c + \tau_c V_c - (\theta_c + \mu + \lambda_c) S_c,\\
\frac{\mathrm{d}V_c}{\mathrm{d}t} &= \theta_c S_c - (1-\epsilon_c)\lambda_c V_c - (\tau_c + \mu) V_c,\\
\frac{\mathrm{d}E_c}{\mathrm{d}t} &= \lambda_c [S_c + (1-\epsilon_c) V_c] - (\sigma_c + \mu) E_c,\\
\frac{\mathrm{d}I_c}{\mathrm{d}t} &= \sigma_c E_c - (\gamma_c + \mu + \delta_c) I_c,\\
\frac{\mathrm{d}R_c}{\mathrm{d}t} &= \gamma_c I_c - (\omega_c + \mu) R_c,
\end{aligned} \tag{3.1}$$

with the following initial condition $S_c(0) > 0, V_c(0) \ge 0, E_c(0) \ge 0, I_c(0) \ge 0, R_c(0) \ge 0$. The total population is given by $N = S_c + V_c + E_c + I_c + R_c$ and the COVID-19 force of infection is given by $\lambda_c = \frac{\beta_c I_c}{N}$.

3.1.1. Boundedness and non-negativity of the solution

In this section, we shall prove the non-negativity and boundedness of the solutions of the ordinary differential equations (ODE) system (3.1). Using the first equation of (3.1) and its positive initial conditions, we shall show that the solution of this system remains positive. We have

$$\begin{aligned}
\frac{\mathrm{d}S_c}{\mathrm{d}t} &= \Lambda + \omega_c R_c + \tau_c V_c - (\theta_c + \mu + \lambda_c) S_c,\\
&\ge \Lambda - (\theta_c + \mu + \lambda_c) S_c.
\end{aligned} \tag{3.2}$$

Since the above ODE is linear and of first-order, the integrating factor is given by

$$U(t) = \exp\left\{ \int_0^t \left[\lambda_c(s) + \theta_c + \mu\right] ds \right\},$$

where $\lambda_c(s) \equiv \lambda_c(S_c, V_c, E_c, I_c, R_c)$. The standard solution of the linear ODE in (3.2) using the integrating factor and ignoring the inequality sign is given by

$$S_c(\xi)\, U(\xi) \Big|_0^t = \Lambda \int_0^t U(\xi)\, \mathrm{d}\xi,$$

which gives

$$\begin{aligned}
&S_c(t) \exp\left\{ \int_0^t \left[\lambda_c(s) + \theta_c + \mu\right] \mathrm{d}s \right\}\\
&\quad \ge S_c(0) + \Lambda \int_0^u \exp\left\{ \int_0^t \left[\lambda_c(s) + \theta_c + \mu\right] \mathrm{d}s \right\} \mathrm{d}u,
\end{aligned}$$

where $S_c(0) \ge 0$, which can easily be simplified to

$$\begin{aligned}
S_c(t) \ge S_c(0) &\exp\left\{ - \int_0^t \left[\lambda_c(s) + \theta_c + \mu\right] \mathrm{d}s \right\}\\
&+ \Lambda \int_0^u \exp\left\{ \int_0^t \left[\lambda_c(s) + \theta_c + \mu\right] \mathrm{d}s \right\} \mathrm{d}u\\
&\times \exp\left\{ - \int_0^t \left[\lambda_c(s) + \theta_c + \mu\right] ds \right\}.
\end{aligned} \tag{3.3}$$

From the above equation, it is guaranteed that $S_c(t)$ is non-negative since $S_c(0)$ and Λ are both positive. From the second equation of (3.1), we have $\dot{V}_c(V_c = 0) = \theta_c S_c$. Since $S_c(0) > 0$ and $S_c(t) \ge 0$, it is guarantee that $V_c(t) \ge 0$ for all $t > 0$. Following the same process, it can be shown that $E_c(t), I_c(t)$ and $R_c(t)$ are all non-negative for all $t > 0$.

We now proceed to prove the boundedness of the solution of Eq. (3.1) at all times $t > 0$. Adding up all equations in (3.1) to have

$$\begin{aligned}
\tfrac{dN_c}{dt} &= \Lambda - \mu(S_c + V_c + E_c + I_c + R_c) - \delta_c I_c\\
&\le \Lambda - \mu N_c \quad \text{since} \quad I_c \ge 0,
\end{aligned}$$

whose solution is given by

$$N_c(t) \le \frac{\Lambda}{\mu} + \left[N_c(0) - \frac{\Lambda}{\mu} \right] e^{-\mu t}.$$

Taking the limit of both sides as $t \to \infty$ gives

$$\lim_{t\to\infty} N_c(t) \leq \frac{\Lambda}{\mu} + \lim_{t\to\infty}\left[\left(N_c(0) - \frac{\Lambda}{\mu}\right)e^{-\mu t}\right] = \frac{\Lambda}{\mu}. \tag{3.4}$$

This result shows that the total COVID-19 population is bounded by Λ/μ for all $t > 0$. More so, we conclude that the ODE system (3.1) is well-posed biologically since all the state variables are non-negative for all $t > 0$.

3.1.2. Disease-free equilibrium and stability analysis

In this subsection, we shall derive the disease-fee equilibrium points, basic reproduction number, and stability properties which are heavily dependent on the value of the reproduction number. The DFE is derived as

$$\zeta_c = (\bar{S}_c, \bar{V}_c, \bar{E}_c, \bar{I}_c, \bar{R}_c) = \left(\frac{\Lambda(\tau_c+\mu)}{\mu(\theta_c+\tau_c+\mu)}, \frac{\Lambda\theta_c}{\mu(\theta_c+\tau_c+\mu)}, 0,\ 0,\ 0\right), \tag{3.5}$$

where $\frac{\bar{S}_c+(1-\epsilon_c)\bar{V}_c}{\bar{N}_c} = \frac{\tau_c+\mu+(1-\epsilon_c)\theta_c}{\theta_c+\tau_c+\mu}$ and $\bar{N}_c = \bar{S}_c + \bar{V}_c = \frac{\Lambda}{\mu}$.

Using the next generation matrix [61,62], the reproduction number is computed and given as

$$R_{cov} = \frac{\sigma_c\beta_c(\tau_c+\mu+(1-\epsilon_c)\theta_c)}{(\sigma_c+\mu)(\gamma_c+\mu+\delta_c)(\theta_c+\tau_c+\mu)}. \tag{3.6}$$

The reproduction number R_{cov} is defined as the average number of new COVID-19 infections generated by a single infection introduced into a susceptible population where a fraction of them are vaccinated. The Theorem 3.1 below explains the condition for the local stability of the DFE points.

Theorem 3.1. *The DFE of the model equation (3.1) is locally asymptotically stable (LAS) if $R_{cov} < 1$, and unstable if $R_{cov} > 1$.*

This theorem implies that COVID-19 can be eliminated from the population when R_{cov} is less than unity if the initial size of the population is under the basin of attraction of the DFE, ζ_c. The proof of Theorem 3.1 is elementary and can be established using Theorem 2 of [63].

3.1.3. Endemic equilibrium and stability analysis

In this subsection, we derive the expressions for the endemic equilibrium points. Due to the complexity and cumbersomeness of the expressions, we consider a limiting ODE model where a vaccinated individual can only get infected with COVID-19 after completely losing their vaccine-induced immunity. In lieu of this, we set $\epsilon_c = 1$ in the model (3.1) for simplification.

The disease-free equilibrium of the reduced model remains the same as that of Eq. (3.1) only that $\frac{\bar{S}_c+(1-\epsilon_c)\bar{V}_c}{\bar{N}_c} = \frac{\tau_c+\mu+(1-\epsilon_c)\theta_c}{\theta_c+\tau_c+\mu}$ becomes $\frac{\bar{S}_c}{\bar{N}_c} = \frac{\tau_c+\mu}{\theta_c+\tau_c+\mu}$. Consequently, the reproduction number (3.6) reduces to

$$R_{covr} = \frac{\theta_c\sigma_c\beta_c(\tau_c+\mu)}{(\sigma_c+\mu)(\gamma_c+\mu+\delta_c)(\theta_c+\tau_c+\mu)}. \tag{3.7}$$

The endemic equilibrium of (3.1) is denoted by ζ_c^* which is represented as

$$\zeta_c^* = (S_c^*, V_c^*, E_c^*, I_c^*, R_c^*), \tag{3.8}$$

and the force of infection at the endemic equilibrium point is given by

$$\lambda_c^* = \frac{\beta_c S_c^*}{N_c^*}. \tag{3.9}$$

Consequently, the state variables at the endemic equilibrium is given by

$$\begin{aligned}
S_c^* &= \frac{\Lambda M_2M_3M_4M_5}{(M_2M_3M_4M_5 - \omega_c\gamma_c\sigma_cM_2)\lambda_c^* + M_1M_2M_3M_4M_5 - \tau_c\theta_cM_3M_4M_5},\\
V_c^* &= \frac{\Lambda M_2M_3M_4M_5\theta_c}{M_2(M_2M_3M_4M_5 - \omega_c\gamma_c\sigma_cM_2)\lambda_c^* + M_1M_2^2M_3M_4M_5 - \tau_c\theta_cM_2M_3M_4M_5},\\
E_c^* &= \frac{\Lambda M_2M_3M_4M_5\lambda_c^*}{M_3(M_2M_3M_4M_5 - \omega_c\gamma_c\sigma_cM_2)\lambda_c^* + M_1M_2M_3^2M_4M_5 - \tau_c\theta_cM_3^2M_4M_5},\\
I_c^* &= \frac{\sigma_c\Lambda M_2M_3M_4M_5\lambda_c^*}{M_3M_4(M_2M_3M_4M_5 - \omega_c\gamma_c\sigma_cM_2)\lambda_c^* + M_1M_2M_3^2M_4^2M_5 - \tau_c\theta_cM_3^2M_4^2M_5},\\
R_c^* &= \frac{\gamma_c\sigma_c\Lambda M_2M_3M_4M_5\lambda_c^*}{M_3M_4M_5(M_2M_3M_4M_5 - \omega_c\gamma_c\sigma_cM_2)\lambda_c^* + M_1M_2M_3^2M_4^2M_5^2 - \tau_c\theta_cM_3^2M_4^2M_5^2},\\
N_c^* &= \frac{\beta_c\sigma_c\Lambda M_2M_3M_4M_5}{M_3M_4(M_2M_3M_4M_5 - \omega_c\gamma_c\sigma_cM_2)\lambda_c^* + M_1M_2M_3^2M_4^2M_5 - \tau_c\theta_cM_3^2M_4^2M_5}.
\end{aligned} \tag{3.10}$$

The expressions in (3.10) are substituted into (3.9) so that the non-zero equilibria satisfy

$$D_1\lambda_c^{*2} + D_2\lambda_c^* + D_3 = 0, \tag{3.11}$$

such that

$$\begin{aligned}
D_1 &= (\Lambda M_3M_4A_2 - \delta_c\sigma_c\Lambda M_2M_3M_4M_5)A_2M_3M_4,\\
D_2 &= M_3^2M_4^2M_5(M_1M_2 - \tau_c\theta_c)(\Lambda M_3M_4A_2 - \delta_c\sigma_cA_1),\\
D_3 &= \Lambda M_3^2M_4^2M_3^2M_4^2M_5^2(M_1M_2 - \tau_c\theta_c)^2(1 - R_{covr}),
\end{aligned}$$

where

$$\begin{aligned}
&M_1 = \theta_c + \mu, M_2 = \tau_c + \mu, M_3 = \sigma_c + \mu, M_4 = \gamma_c + \mu + \delta_c,\\
&M_5 = \omega + \mu, \rho_c = 1 - \epsilon_c,
\end{aligned}$$

$$A_1 = \Lambda M_2M_3M_4M_5, A_2 = M_2(M_3M_4M_5 - \omega_c\gamma_c\sigma_c).$$

By expansion and factorization, it can be seen that the sign of D_1 is positive explicitly. The sign of D_2 cannot be explicitly determined because of the negative sign but $D_3 \geq 0$ if and only if $R_{covr} \leq 1$. The endemic equilibrium (equilibria) of the model can be obtained by solving for the positive values of λ_c^* in (3.11) and substituting it into (3.10). These equilibria exist for $\lambda_c^* > 1$ and are summarized in the following theorem.

Theorem 3.2. *The ODE model (3.1) has*

i. a unique endemic equilibrium if $D_3 < 0 \iff R_{covr} > 1$;
ii. a unique endemic equilibrium if $D_2 < 0$ and $D_3 = 0$ or $D_2^2 - 4D_1D_3 = 0$;
iii. two endemic equilibria if $D_3 > 0$, $D_2 < 0$ and $D_2^2 - 4D_1D_3 > 0$;
iv. no endemic equilibrium otherwise.

In Theorem 3.2, case (*ii*) shows the existence of an endemic equilibrium but the expression of D_2 is not explicitly negative and D_3 is not equal to zero (only if $R_{covr} = 1$). For the case (*iii*), though $D_3 > 0$ if $R_{covr} < 1$ but D_2 is not explicitly negative and $D_2^2 - 4D_1D_3$ will contain some negative and positive terms which will make the condition $D_2^2 - 4D_1D_3 > 0$ difficult to satisfy. For this reason, the easiest conclusion we can make is that the model (3.1) satisfies case (*i*) (which means that the endemic equilibrium exists when the reproduction number R_{covr}, is greater than 1). The existence of backward bifurcation in case (*iii*) is also possible. Hence, we have the following theorem.

Theorem 3.3. *The endemic equilibrium of the model equation (3.1) (under the condition that $\epsilon_c = 1$) is locally asymptotically stable (LAS) if $R_{covr} > 1$, and unstable if $R_{covr} < 1$.*

This theorem implies that COVID-19 can be eliminated from the population when the threshold parameter $R_{covr} < 1$ if the initial size of the population is under the basin of attraction of the DFE, ζ_c. The proof

of Theorem 3.3 is elementary and can be established using Theorem 2 of [63].

3.2. Analysis of the influenza sub-model

For the influenza sub-model, we shall set all COVID-19 and co-infection-related parameters and variables to zero. These variables are $V_c = V_{ci} = R_c = R_{ci} = I_c = I_{ci} = E_c = E_{ci} = 0$ and the parameters include $\beta_c = \beta_{ci} = \tau_c = \tau_{ci} = \omega_c = \omega_{ci} = \delta_c = \delta_{ci} = 0$ among others. The influenza sub-model is given by

$$\begin{aligned}
\frac{\mathrm{d}S_i}{\mathrm{d}t} &= \Lambda + \omega_i R_i + \tau_i V_i - (\theta_i + \mu + \lambda_i) S_i,\\
\frac{\mathrm{d}V_i}{\mathrm{d}t} &= \theta_i S_i - (1-\epsilon_i)\lambda_i V_i - (\tau_i + \mu) V_i,\\
\frac{\mathrm{d}I_i}{\mathrm{d}t} &= \lambda_i [S_i + (1-\epsilon_i) V_i] - (\gamma_i + \delta_i + \mu) I_i,\\
\frac{\mathrm{d}R_i}{\mathrm{d}t} &= \gamma_i I_i - (\omega_i + \mu) R_i,
\end{aligned} \tag{3.12}$$

with the following initial conditions $S_i(0) > 0, V_i(0) \geq 0, I_i(0) \geq 0, R_i(0) \geq 0$. The total population is given by $N = S_i + V_i + I_i + R_i$ and the influenza force of infection is given by $\lambda_i = \frac{\beta_i I_i}{N}$.

3.2.1. Boundedness and non-negativity of the solution

In this section, we shall prove the non-negativity and boundedness of the solutions of the ODE system (3.12). Using the first equation of (3.12) and its positive initial conditions, we shall show that the solution of this system remains positive. We have

$$\begin{aligned}
\frac{\mathrm{d}S_i}{\mathrm{d}t} &= \Lambda + \omega_i R_i + \tau_i V_i - (\theta_i + \mu + \lambda_i) S_i,\\
&\geq \Lambda - (\theta_i + \mu + \lambda_i) S_i.
\end{aligned} \tag{3.13}$$

Since the above ODE is linear and of first-order, the integrating factor is given by

$$Q(t) = \exp\left\{ \int_0^t \left[\lambda_i(s) + \theta_i + \mu\right] \, ds \right\},$$

where $\lambda_i(s) \equiv \lambda_i(S_i, V_i, E_i, I_i, R_i)$. The standard solution of the linear ODE in (3.13) using the integrating factor and ignoring the inequality sign is given by

$$S_i(\eta)\, Q(\eta) \,\big|_0^t = \Lambda \int_0^t Q(\eta) \, \mathrm{d}\eta,$$

which gives

$$\begin{aligned}
&S_i(t) \, \exp\left\{ \int_0^t \left[\lambda_i(s) + \theta_i + \mu\right] \, \mathrm{d}s \right\}\\
&\quad \geq S_i(0) + \Lambda \int_0^u \exp\left\{ \int_0^t \left[\lambda_i(s) + \theta_i + \mu\right] \, \mathrm{d}s \right\} \, \mathrm{d}u,
\end{aligned}$$

where $S_i(0) \geq 0$, which can easily be simplified to

$$\begin{aligned}
S_i(t) \geq S_i(0) &\exp\left\{ - \int_0^t \left[\lambda_i(s) + \theta_i + \mu\right] \, \mathrm{d}s \right\}\\
&+ \Lambda \int_0^u \exp\left\{ \int_0^t \left[\lambda_i(s) + \theta_i + \mu\right] \, \mathrm{d}s \right\} \, \mathrm{d}u\\
&\times \exp\left\{ - \int_0^t \left[\lambda_i(s) + \theta_i + \mu\right] ds \right\}.
\end{aligned} \tag{3.14}$$

From the above equation, it is guaranteed that $S_i(t)$ is non-negative since $S_i(0)$ and Λ are both positive. From the second equation of (3.12), we have $\dot{V}_i(V_i = 0) = \theta_i S_i$. Since $S_i(0) > 0$ and $S_i(t) \geq 0$, it is guarantee that $V_i(t) \geq 0$ for all $t > 0$. Following the same process, it can be shown that $I_i(t)$ and $R_i(t)$ are all non-negative for all $t > 0$.

We now proceed to prove the boundedness of the solution of Eq. (3.12) at all times $t > 0$. Adding up all equations in (3.12) to have

$$\begin{aligned}
\frac{dN_i}{dt} &= \Lambda - \mu(S_i + V_i + I_i + R_i) - \delta_i I_i\\
&\leq \Lambda - \mu N_i \quad \text{since} \quad I_i \geq 0,
\end{aligned}$$

whose solution is given by

$$N_i(t) \leq \frac{\Lambda}{\mu} + \left[N_i(0) - \frac{\Lambda}{\mu} \right] e^{-\mu t}.$$

Taking the limit of both sides as $t \to \infty$ gives

$$\lim_{t\to\infty} N_i(t) \leq \frac{\Lambda}{\mu} + \lim_{t\to\infty} \left[\left(N_i(0) - \frac{\Lambda}{\mu} \right) e^{-\mu t} \right] = \frac{\Lambda}{\mu}. \tag{3.15}$$

This result shows that the total COVID-19 population is bounded by Λ/μ for all $t > 0$. More so, we conclude that the ODE system (3.12) is well-posed biologically since all the state variables are non-negative for all $t > 0$.

3.2.2. Disease-free equilibrium and stability analysis

In this subsection, we shall derive the disease-fee equilibrium points, basic reproduction number, and stability properties which are heavily dependent on the value of the reproduction number. The DFE is derived as

$$\zeta_i = (\bar{S}_i, \bar{V}_i, \bar{I}_i, \bar{R}_i) = \left(\frac{\Lambda(\tau_i + \mu)}{\mu(\theta_i + \tau_i + \mu)}, \frac{\Lambda\theta_i}{\mu(\theta_i + \tau_i + \mu)}, 0,\ 0,\ 0 \right), \tag{3.16}$$

where $\frac{\bar{S}_i + (1-\epsilon_i)\bar{V}_i}{\bar{N}_i} = \frac{\tau_i + \mu + (1-\epsilon_i)\theta_i}{\theta_i + \tau_i + \mu}$ and $\bar{N}_i = \bar{S}_i + \bar{V}_i = \frac{\Lambda}{\mu}$.

Using the next generation matrix [61,62], the reproduction number is computed as

$$R_{inf} = \frac{\beta_i(\tau_i + \mu + (1-\epsilon_i)\theta_i)}{(\gamma_i + \mu + \delta_i)(\theta_i + \tau_i + \mu)}. \tag{3.17}$$

The reproduction number R_{inf} is defined as the average number of new influenza infections generated by a single infection introduced into a susceptible population where a fraction of them are vaccinated. The theorem below explains the condition for the local stability of the DFE points.

Theorem 3.4. *The DFE of the model equation (3.12) is locally asymptotically stable (LAS) if $R_{inf} < 1$, and unstable if $R_{inf} > 1$.*

This theorem implies that influenza can be eliminated from the population when R_{inf} is less than unity if the initial size of the population is under the basin of attraction of the DFE, ζ_i. The proof of Theorem 3.4 is elementary and can be established using Theorem 2 of [63].

3.2.3. Endemic equilibrium and stability analysis

In this subsection, we derive the expressions for the endemic equilibrium points. Due to the complexity and cumbersomeness of the expressions, we consider a limiting ODE model where a vaccinated individual can only get infected with influenza after completely losing their vaccine-induced immunity. In lieu of this, we set $\epsilon_i = 1$ in the model (3.12) for simplification.

The disease-free equilibrium of the reduced model remains the same as that of Eq. (3.12) only that $\frac{\bar{S}_i + (1-\epsilon_i)\bar{V}_i}{\bar{N}_i} = \frac{\tau_i + \mu + (1-\epsilon_i)\theta_i}{\theta_i + \tau_i + \mu}$ becomes $\frac{\bar{S}_i}{\bar{N}_i} = \frac{\tau_i + \mu}{\theta_i + \tau_i + \mu}$. Consequently, the reproduction number (3.17) reduces to

$$R_{infr} = \frac{\beta_i(\tau_i + \mu)}{(\gamma_i + \mu + \delta_i)(\theta_i + \tau_i + \mu)}. \tag{3.18}$$

The endemic equilibrium of (3.12) is denoted by ζ_i^* which is represented as

$$\zeta_i^* = (S_i^*, V_i^*, I_i^*, R_i^*), \tag{3.19}$$

and the force of infection at the endemic equilibrium point is given by

$$\lambda_i^* = \frac{\beta_i S_i^*}{N_i^*}. \tag{3.20}$$

Consequently, the state variables at the endemic equilibrium is given by

$$S_i^* = \frac{\Lambda B_2 B_3 B_4}{B_2(B_3B_4 - \omega_i\gamma_i)\lambda_i + B_3B_4(B_1B_2 - \tau_i\theta_i)},$$
$$V_i^* = \frac{\Lambda B_2 B_3 B_4\theta_i}{B_2^2(B_3B_4 - \omega_i\gamma_i)\lambda_i + B_2B_3B_4(B_1B_2 - \tau_i\theta_i)},$$
$$I_i^* = \frac{\Lambda B_2 B_3 B_4\lambda_i}{B_2B_3(B_3B_4 - \omega_i\gamma_i)\lambda_i + B_3^2B_4(B_1B_2 - \tau_i\theta_i)},$$
$$R_i^* = \frac{\Lambda B_2 B_3 B_4\gamma_i\lambda_i}{B_2B_3B_4(B_3B_4 - \omega_i\gamma_i)\lambda_i + B_3^2B_4^2(B_1B_2 - \tau_i\theta_i)},$$
$$N_i^* = \frac{(\Lambda B_3B_2(B_3B_4 - \omega_i\gamma_i) - \mu\delta_i\Lambda B_2B_3B_4)\lambda_i^* + \Lambda B_3^2B_4(B_3B_4 - \omega_i\gamma_i)}{\mu(B_2B_3(B_3B_4 - \omega_i\gamma_i)\lambda_i + B_3^2B_4(B_1B_2 - \tau_i\theta_i))}. \tag{3.21}$$

The expressions in (3.21) are substituted into (3.20) so that the non-zero equilibria satisfy

$$D_4\lambda_i^* + D_5 = 0, \tag{3.22}$$

such that

$$D_4 = \mu\gamma_i + \omega_i\delta_i(1-\mu) + \mu\delta_i(1-\mu),$$
$$D_5 = \Lambda\mu(\gamma_i + \delta_i + \mu)^2(\omega_i + \mu)(\tau_i + \theta_i + \mu)(1 - R_{infr}).$$

Clearly, $D_4 > 0$ since $0 < \mu < 1$ and $D_5 \geq 0$ whenever $R_{infr} \leq 1$ so that $\lambda_c^* = -\frac{D_5}{D_4}$ for $R_{infr} < 1$.

Therefore, for this case, the linear equation in (3.22) has no positive solution and as such, has no positive endemic equilibrium whenever $R_{infr} < 1$. In this case, the possibility of backward bifurcation is consequently ruled out. This is because bifurcation only occurs when at least two positive endemic equilibria exist whenever $R_{infr} < 1$ [49,64,65].

Hence, we have the following theorem.

Theorem 3.5. *The endemic equilibrium of the model equation (3.12) (under the condition that $\epsilon_i = 1$) is locally asymptotically stable (LAS) if $R_{infr} > 1$, and unstable if $R_{infr} < 1$.*

This theorem implies that influenza can be eliminated from the population when the threshold parameter $R_{infr} < 1$ if the initial size of the population is under the basin of attraction of the DFE, ζ_i. The proof of Theorem 3.5 is elementary and can be established using theorem 2 of [63].

3.3. Analysis of the co-infection model

Here, we shall discuss the boundedness and positivity of solution of the co-infection model (2.15). Following the approach in the previous subsections, it can be shown that the solution of (2.15) is non-negative and that the solution is bounded in the feasible region $\Theta \subset \mathcal{R}_+^{12}$ such that

$$\Theta = \{(S, V_c, E_c, I_c, R_c, V_i, I_i, R_i, V_{ci}, E_{ci}, I_{ci}, R_{ci}) \in \mathcal{R}_+^{12} : N \leq N(0)\},$$

where $N = S + V_c + E_c + I_c + R_c + V_i + I_i + R_i + V_{ci} + E_{ci} + I_{ci} + R_{ci}$. In this regard, the co-infection model (2.15) is mathematically and epidemiologically well-posed in the feasible region Θ and the solutions are non-negative.

The disease-free equilibrium, ζ_0, is given by

$$\begin{aligned}\zeta_0 &= (\bar{S}_0, \bar{V}_{i0}, \bar{V}_{c0}, \bar{V}_{ci0}, \bar{E}_{c0}, \bar{I}_{c0}, \bar{R}_{c0}, \bar{I}_{i0}, \bar{R}_{i0}, \bar{E}_{ci0}, \bar{I}_{ci0}, \bar{R}_{ci0})\\ &= \left(\bar{S}_0, \bar{V}_{i0}, \bar{V}_{c0}, \bar{V}_{ci0}, 0, 0, 0, 0, 0, \ 0, \ 0, 0\right),\end{aligned} \tag{3.23}$$

where

$$\bar{S}_0 = \frac{\Lambda(\tau_c + \mu)(\tau_i + \mu)(\tau_{ci} + \mu)}{\mu[(\tau_i + \mu)(\tau_{ci} + \mu)\theta_c + (\tau_c + \mu)(\tau_{ci} + \mu)\theta_i + (\tau_i + \mu)(\tau_c + \mu)\theta_{ci}]},$$
$$\bar{V}_{c0} = \frac{\theta_c\Lambda(\tau_{ci} + \mu)(\tau_i + \mu)}{\mu[(\tau_i + \mu)(\tau_{ci} + \mu)\theta_c + (\tau_c + \mu)(\tau_{ci} + \mu)\theta_i + (\tau_i + \mu)(\tau_c + \mu)\theta_{ci}]},$$
$$\bar{V}_{i0} = \frac{\theta_i\Lambda(\tau_{ci} + \mu)(\tau_c + \mu)}{\mu[(\tau_i + \mu)(\tau_{ci} + \mu)\theta_c + (\tau_c + \mu)(\tau_{ci} + \mu)\theta_i + (\tau_i + \mu)(\tau_c + \mu)\theta_{ci}]},$$
$$\bar{V}_{ci0} = \frac{\theta_{ci}\Lambda(\tau_c + \mu)(\tau_i + \mu)}{\mu[(\tau_i + \mu)(\tau_{ci} + \mu)\theta_c + (\tau_c + \mu)(\tau_{ci} + \mu)\theta_i + (\tau_i + \mu)(\tau_c + \mu)\theta_{ci}]},$$

and $\bar{N}_0 = \bar{S}_0 + \bar{V}_{i0} + \bar{V}_{c0} + \bar{V}_{ci0} = \frac{\Lambda}{\mu}$. Using the next generation matrix [61,62], the reproduction number for (2.15) is computed as

$$R_{cof} = \max\{R_{cov}, R_{inf}\}, \tag{3.24}$$

where R_{cov} and R_{inf} are as given in Eqs. (3.6) and (3.17) respectively. Hence, the following result follows.

Theorem 3.6. *The DFE of the model equation (2.15) is locally asymptotically stable (LAS) if $R_{cof} < 1$, and unstable if $R_{cof} > 1$.*

4. Numerical simulation using the demography of Israel

Numerical simulations of the sub-models and the co-infection model are performed to give a broad view of the time evolution of the infected populations. It will also serve as a tool to understand the dynamics of the model and a technique to investigate the significance of some important parameters of the model. The model simulation results shall help to validate the potential benefits of different vaccination programs when implemented concurrently or separately in controlling both COVID-19 and influenza diseases. The contribution of the immunity waning rates as well as the vaccine efficacy rates shall also be investigated.

Based on the projections of the 2022 United Nations data [59], the current population of Israel is 9,103,434 which represents 0.11% of the world population. This makes the total population $N(0) =$ 9,103,434. Since it is difficult to differentiate between the total COVID-19 population N_c and the influenza population N_i, we set $N_c(0) = N_i(0) = N(0)$. According to [66], the total COVID-19 confirmed cases in Israel is 4,760,050, we assume that the initial infected population at the beginning of this modeling study is given by $I_c(0) =$ 1,428,015 which is 30% of 4,760,050. The total number of recovered persons, R_c, is given by 4,735,805 [66], it is assumed that the initial recovered population at the beginning of the modeling study is given by 30% of 4,735,050 which is $R_c(0) =$ 1,420,742. At April 3, 2021, [67] reported that 4,714,932 which is 72.1% of 6 538 911 people aged 16 years and older were fully vaccinated with two doses of BNT162b.

We set the initial vaccinated population to $V_c(0) =$ 1,414,480. Since there is no data for the initial number of the exposed population, we set $E_c(0) =$ 300,000. The susceptible population is calculated using the formula

$$S(0) = N(0) - (I_c(0) + V_c(0) + E_c(0) + R_c(0)) = 4{,}540{,}197.$$

The detailed initial conditions are given in Table 3. According to the world population [59], the current median age in Israel is approximately 29.9, with a total life expectancy of 82.5 years of age. The natural death rate is defined as the reciprocal of the total life expectancy. Hence, $\mu = \frac{1}{82.5} = 0.0121$ per year. In 2021, the total number of people that migrated to Israel was 27,050 [50] while the current birth rate for Israel in 2022 is 19.248 births per 1000 people [51]. With this, we estimate $\Lambda =$ 52,272. Other parameter values can be found on Table 2.

5. Discussion of results

In Fig. 2, the numerical solution of the model (3.1) for the disease-free equilibrium is presented. The initial conditions used are as presented in Table 3. The vaccination rate used is $\theta_c = 0.8500$ with $\epsilon_c = 0.9050$ efficacy rate. The vaccine and post-recovery immunity waning rates are $\tau_c = 0.15$, $\omega_c = 0.15$, corresponding to a reproduction number of $R_{cov} = 0.8278$ which is less than unity. All other parameters

Table 3
Model initial conditions. These initial conditions are based on the Israeli statistics as of December 29, 2022. The influenza susceptible population is computed using $S_i(0) = N_i(0) - (V_i(0) + I_i(0) + R_i(0))$ while the co-infection susceptible population is computed using $S_{ci}(0) = N_{ci}(0) - (V_{ci}(0) + E_{ci}(0) + I_{ci}(0) + R_{ci}(0))$. The initial conditions used for the influenza population are inferred from the Israeli center for disease control ICDC [68].

Variable	Value	References
$N(0) = N_i(0) = N_c(0) = N_{ci}(0)$	9,103,434	[59]
$S_c(0)$	4,540,197	Computed from [59]
$S_i(0)$	4,701,979	[67]
$V_c(0)$	1,414,480	[67]
$I_c(0)$	1,428,015	[66]
$E_c(0)$	300,000	Assumed
$R_c(0)$	1,420,742	[66]
$V_i(0)$	1,700,000	2017/2018 influenza data [68]
$I_i(0)$	1455	2017/2018 influenza data [68]
$R_i(0)$	2,700,000	Inferred from 2017/2018 influenza data [68]
$S_{ci}(0)$	4,403,433	Assumed
$V_{ci}(0)$	1,700,000	Assumed
$E_{ci}(0)$	300,000	Assumed
$I_{ci}(0)$	1	[69]
$V_{ci}(0)$	2,700,000	Assumed

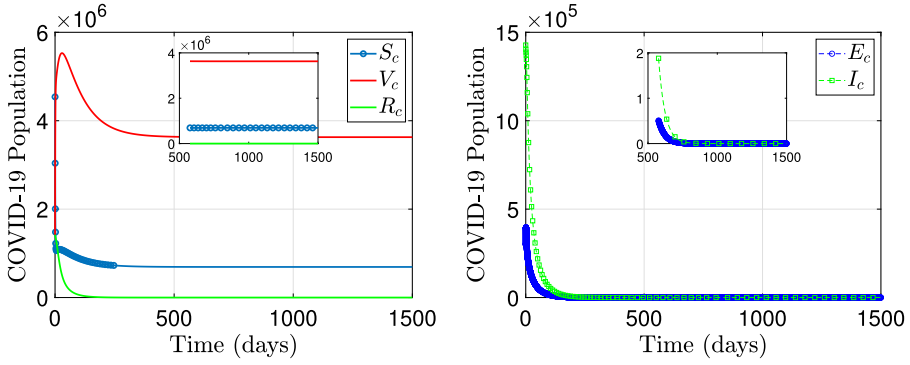

Fig. 2. Disease-free dynamics. The time COVID-19 dynamics of the susceptible (S_c), vaccinated (V_c) and recovered (R_c) populations (left panel), and those for the exposed (E_c) and infectious (I_c), populations (right panel), showing the disease-free equilibrium dynamics. Vaccination rate is $\theta_c = 0.8500$, with vaccine efficacy, $\epsilon_c = 0.8900$. The vaccine and post-recovery immunity waning rates are $\tau_c = 0.15$, $\omega_c = 0.15$, corresponding to a reproduction number of $R_{cov} = 0.8278$. All other parameters are as given in Table 2.

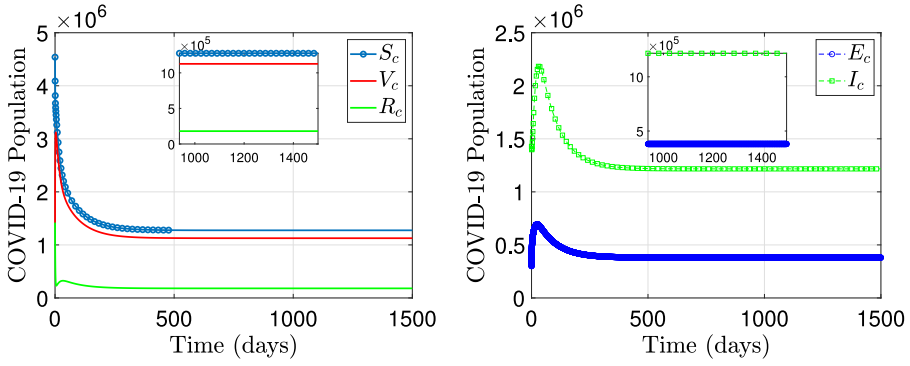

Fig. 3. Endemic dynamics. The COVID-19 time dynamics of the susceptible (S_c), Vaccinated (V_c) and recovered (R_c) populations (left panel), and the exposed (E_c) and infectious (I_c) populations (right panel), for when the disease is endemic in the population. The Vaccination rate is $\theta_c = 0.8500$, with vaccine efficacy, $\epsilon_c = 1$. The vaccine and post-recovery immunity waning rates are $\tau_c = \omega_c = 0.95$, corresponding to a reproduction number of $R_{covr} = 1.7403$. All other parameters are given in Table 2.

are as given in Table 2. It can be observed from the results in the right panel that the infected populations diminish steadily toward zero within the first 250 days while the uninfected populations S_c, V_c (see left panel) increase steadily and later stabilize at the top. The recovered population R_c decreases steadily as expected. These results validate the statement of Theorem 3.1 which means that whenever the COVID-19 reproduction number becomes less than 1, the disease dies out, and both the susceptible and vaccinated populations become stable. It also means that if the average number of new COVID-19 infections generated by a single infection introduced into a susceptible population in any province in Israel is less than 1, then the COVID-19 virus will be eliminated in the population within 250 days. In Fig. 3, we increased the waning rates to $\tau_c = \omega_c = 0.95$ and $\epsilon_c = 1$ while $\beta_c = 0.8520$. Other parameter values remain the same. The corresponding value of the reproduction number is $R_{conr} = 1.7403$. It can be observed from the right panel that the infected populations increase and remain stable for 1500 days and beyond. On the left panel, the recovered population increases because of the endemic state of the disease while both susceptible and vaccinated populations reduce drastically, but do not tend to zero. This result shows that the DFE is unstable when $R_{covr} > 1$, and as a result, the disease cannot be eliminated from the population. It also means that if the average number of new COVID-19

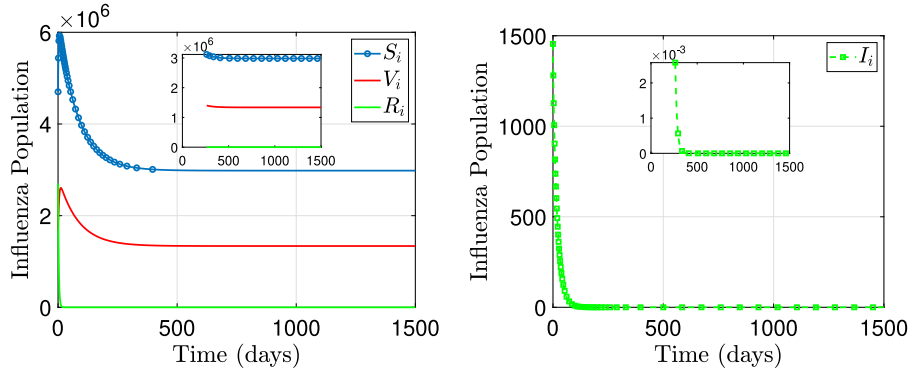

Fig. 4. Disease-free dynamics. The time influenza dynamics of the susceptible (S_i), vaccinated (V_i), and recovered (R_i) populations (left panel), and the infected (I_i), populations (right panel), showing the disease-free equilibrium dynamics. Vaccination rate is $\theta_i = 0.1485$, with vaccine efficacy, $\epsilon_i = 0.8900$. The vaccine and post-recovery immunity waning rates are $\tau_i = 0.3190$, $\omega_i = 0.3190$ respectively, corresponding to a reproduction number of $R_{inf} = 0.7869$. All other parameters are as given in Table 2.

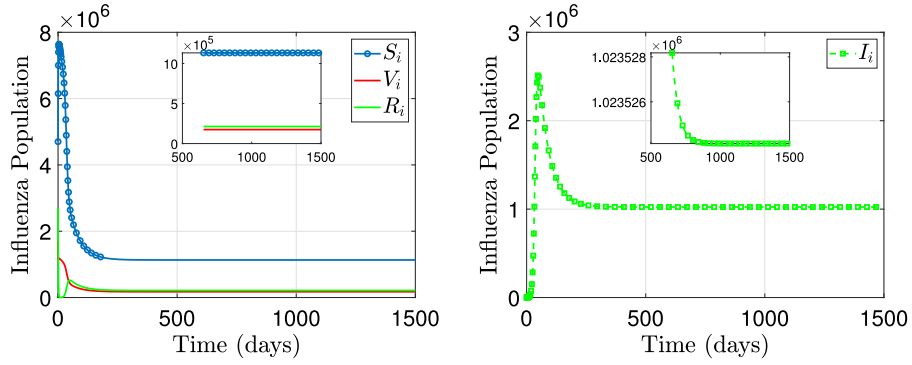

Fig. 5. Endemic dynamics. The influenza time dynamics of the susceptible (S_i), Vaccinated (V_i), and recovered (R_i) populations (left panel), and the infected (I_i) populations (right panel), for when the disease is endemic in the population. The Vaccination rate is $\theta_i = 0.1485$, with vaccine efficacy, $\epsilon_i = 1$. The vaccine and post-recovery immunity waning rates are $\tau_i = \omega_i = 0.95$ and $\beta_i = 0.5230$, corresponding to a reproduction number of $R_{infr} = 1.9453$. All other parameters are given in Table 2.

infections generated by a single infection introduced into a susceptible population in any province in Israel is greater than 1, then the COVID-19 virus will remain in the population for a longer time. In Fig. 5, we increased the waning rates to $\tau_i = \omega_i = 0.95$ and $\epsilon_i = 1$ while other parameter values remain the same. The corresponding value of the reproduction number is $R_{infr} = 1.9453$. It can be observed from the right panel that the infected population increases and remain stable for 1500 days and beyond. On the left panel, the recovered population increases because of the endemic state of the disease while both susceptible and vaccinated populations reduced drastically but do not tend to zero. This result shows that the DFE is unable when $R_{infr} > 1$, and as a result, the disease cannot be eliminated from the population. It also means that if the average number of new influenza infections generated by a single infection introduced into a susceptible population in any province in Israel is greater than 1, then the influenza virus will remain in the population for a longer time. In Fig. 4, the numerical solution of the model (3.12) for the disease-free equilibrium is presented. The initial conditions used are as presented in Table 3. The vaccination rate used is $\theta_i = 0.1485$ with $\epsilon_i = 0.8900$ efficacy rate. The effective contact rate $\beta_i = 0.2530$. The vaccine and post-recovery immunity waning rates are $\tau_i = 0.3190$, $\omega_i = 0.3190$, corresponding to a reproduction number of $R_{inf} = 0.7869$ which is less than unity. All other parameters are as given in Table 2. It can be observed from the results in the right panel that the infected populations diminish steadily toward zero within the first 250 days while the uninfected populations S_i, V_i (see left panel) increase steadily and later stabilize at the top. The recovered population R_i decreases steadily as expected. These results validate the statement of Theorem 3.4 which means that whenever the influenza reproduction number becomes less than 1, the disease dies out, and both the susceptible and vaccinated populations become stable. It also means that if the average number of new influenza infections generated by a single infection introduced into a susceptible population in any province in Israel is less than 1, then the influenza virus will be eliminated in the population within 250 days.

Fig. 6 shows the dynamics of the COVID-19 population over time as the immunity waning rates increase. In the left panel, for the waning rates $\omega_c = 0.25, 0.50, 0.75$, and 0.90, the corresponding reproduction number is $R_{cov} = 2.1285$ for all values of ω_c. The vaccination, vaccine efficacy, and vaccine-induced immunity waning rates used are $\theta_c = 0.5, \epsilon_c = 0.85$, and $\tau_c = 0.7$ respectively. Other parameter values are in Table 2. The COVID-19 epidemic peak is approximate 11.4×10^6 and later stable around 1.5×10^6 for the highest value of the waning rate $\omega_c = 0.9$. In the right panel, when the values of vaccine-immunity waning rate are $0.25, 0.50, 0.75$, and 0.90, the corresponding values of R_{cov} are $1.4498, 1.9014, 2.1740$ and 2.2912. The parameter values used are the same as the left panel. Other parameter values are in Table 2. The COVID-19 epidemic peak is approximate 2.4×10^6 and later stable around 1.2×10^6 for the highest value of the waning rate $\tau_c = 0.9$. It is also observed from Fig. 6 that the post-recovery waning rate has lesser effects on the disease dynamics compared to the vaccine-induced immunity waning rate. One of the reasons for this observation is that the COVID-19 reproduction number R_{cov} does not depend on the parameter ω_c because the value of R_{cov} remains constant for all values of ω_c thereby showing lesser effects on the dynamics of the disease. The result is completely different from the one on the right panel. The values of R_{cov} increase with an increase in τ_c and the disease prevalence in the population increases as more people lose their vaccine-induced immunity. Similar results are obtained in Fig. 7 and the same explanation holds for the dynamics of the influenza population. The influenza dynamics peak in the left panel is approximate 1.88×10^6 and later

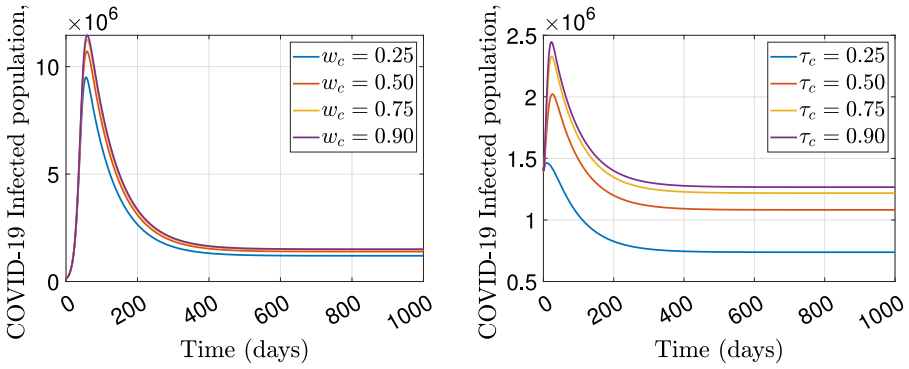

Fig. 6. COVID-19 epidemic peak for varying immunity waning rates. The dynamics of the COVID-19 population over time for different post-recovery immunity waning rates (left panel) and vaccine-induced immunity waning rates (right panel). In the left panel, for the waning rates $\omega_c = 0.25, 0.50, 0.75$, and 0.90, the corresponding reproduction number is $R_{cov} = 2.1285$ for all values of ω_c. The vaccination, vaccine efficacy, and vaccine-induced immunity waning rates used are $\theta_c = 0.5, \epsilon_c = 0.85$, and $\tau_c = 0.7$ respectively. Other parameter values are in Table 2. In the right panel, when the values of vaccine-immunity waning rate are $0.25, 0.50, 0.75$, and 0.90, the corresponding values of R_{cov} are $1.4498, 1.9014, 2.1740$ and 2.2912 respectively. The parameter values used are the same as the left panel. Other parameter values are in Table 2.

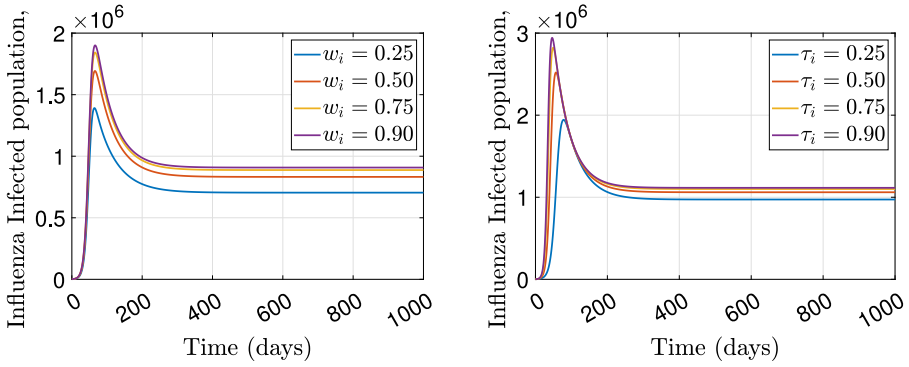

Fig. 7. Influenza dynamics peak for varying immunity waning rates. The dynamics of the influenza population over time for different post-recovery immunity waning rates (left panel) and vaccine-induced immunity waning rates (right panel). In the left panel, for the waning rates $\omega_i = 0.25, 0.50, 0.75$, and 0.90, the corresponding reproduction number is $R_{inf} = 1.6554$ for all values of ω_i. The vaccination rate, vaccine efficacy, and vaccine-induced immunity waning used are $\theta_i = 0.5, \epsilon_i = 0.65$ and $\tau_i = 0.7$ respectively. Other parameter values are in Table 2. In the right panel, when the values of vaccine-immunity waning rate are $0.25, 0.50, 0.75$, and 0.90, the corresponding values of R_{inf} are $1.7221, 2.0341, 2.2225$ and 2.3036 respectively. The parameter values used are the same as the left panel. Other parameter values are in Table 2.

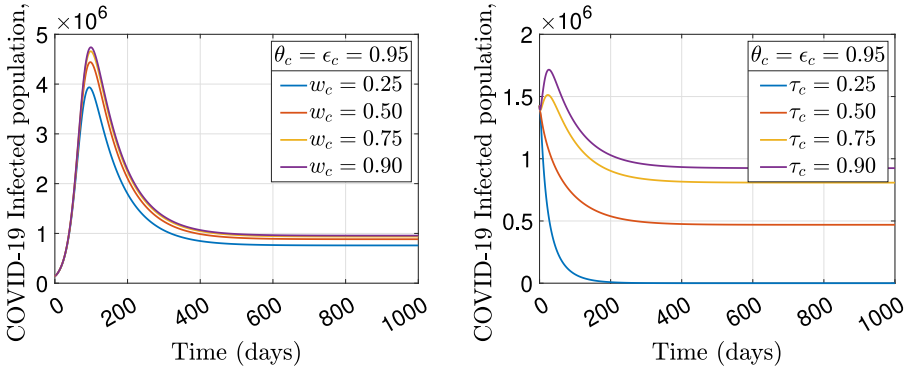

Fig. 8. COVID-19 epidemic peak for varying vaccination and vaccine efficacy rates. The dynamics of the COVID-19 population over time for different vaccination and vaccine efficacy rates under post-recovery immunity waning rates(left panel) and vaccine-induced immunity waning rates (right panel). In the left panel, for the vaccination and vaccine efficacy rates $\theta_c = \epsilon_c = 0.95$, the corresponding reproduction number is $R_{cov} = 1.4980$ for all values of ω_c while $\tau_c = 0.7$. Other parameter values are in Table 2. In the right panel, for the vaccination and vaccine efficacy rates $\theta_c = \epsilon_c = 0.95$, the corresponding values of R_{cov} are 0.8372, 1.2545, 1.5499, and 1.6891 respectively. Other parameter values are in Table 2.

stable around 0.98×10^6 for the highest value of the waning rate $\omega_i = 0.9$. The influenza dynamics peak in the right panel is approximate 2.6×10^6 and later stable around 1.08×10^6 for the highest value of the waning rate $\tau_i = 0.9$.

Fig. 8 shows the dynamics of the COVID-19 population over time as the vaccination and vaccine efficacy rates increase. In the left panel, for the vaccination and vaccine efficacy rates $\theta_c = \epsilon_c = 0.95$, the corresponding reproduction number is $R_{cov} = 1.498$ for all values of ω_c and $\tau_c = 0.7$. Other parameter values are in Table 2. The COVID-19 epidemic peak reduced approximately to 4.7×10^6 and later stable around 0.95×10^6 for the highest value of the waning rate $\omega_c = 0.9$. In the right panel, when the vaccination and vaccine efficacy rates are $\theta_c = \epsilon_c = 0.95$, the corresponding values of R_{cov} are 0.8372, 1.2545, 1.5499, and 1.6891. Other parameter values are in Table 2. The COVID-19

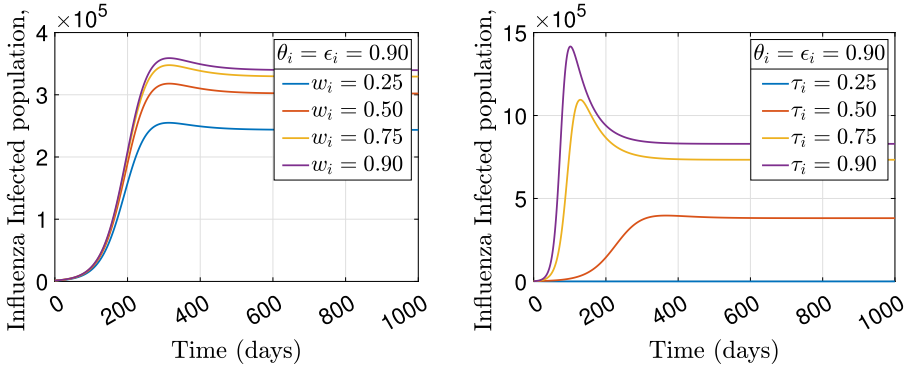

Fig. 9. Influenza dynamics peak for varying vaccination and vaccine efficacy rates. The dynamics of the influenza population over time for different vaccination and vaccine efficacy rates under post-recovery immunity waning rates (left panel) and vaccine-induced immunity waning rates (right panel). In the left panel, for the vaccination and vaccine efficacy rates $\theta_i = \epsilon_i = 0.90$, the corresponding reproduction number is $R_{inf} = 1.1222$ for all values of ω_i, while $\tau_i = 0.7$. Other parameter values are in Table 2. In the right panel, for the vaccination and vaccine efficacy rates $\theta_i = \epsilon_i = 0.90$, the corresponding values of R_{inf} are $0.7625, 1.1426, 1.4117$ and 1.5385 respectively. Other parameter values are in Table 2.

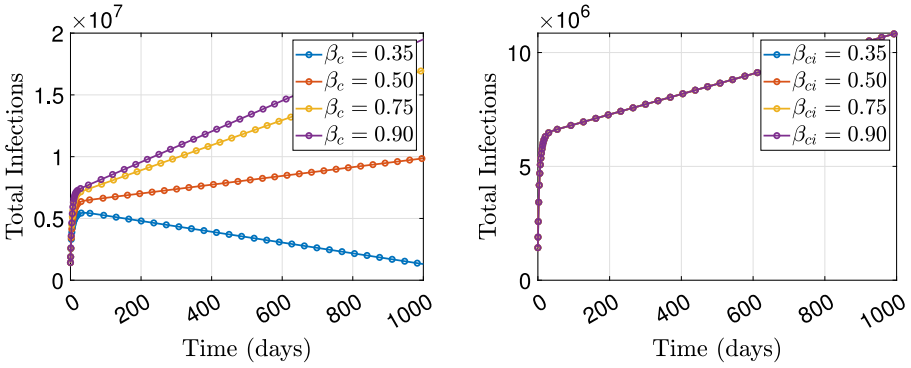

Fig. 10. Effects of the contact rates on the co-infection dynamics. The dynamics of the co-infection population over time for different values of the COVID-19 effective contact rates (left panel) and different values of co-infection contact rates (right panel). In both panels, $\epsilon_{ci} = \epsilon_i = \epsilon_c = 0.6$, $\theta_i = \theta_{ci} = \theta_c = 0.45$, $\omega_c = \omega_i = \omega_{ci} = \tau_i = \tau_c = \tau_{ci} = 0.85$. Other parameter values are in Table 2.

epidemic peak reduced approximately to 1.7×10^6 and later stable around 0.95×10^6 for the highest value of the waning rate $\tau_c = 0.9$. It is also observed from Fig. 8 that the vaccination and vaccine efficacy rates have significant effects on the disease dynamics as the reproduction number reduced drastically from its previous value. Although the reproduction number is still greater than unity, this is because the effects of post-recovery rates are not felt in the reproduction number. The result on the right panel is more promising than that of the left panel. The values of R_{cov} decrease with an increase in θ_c, ϵ_c, and the disease prevalence in the population decrease as more people get vaccinated. The COVID-19 epidemic peak reduced approximately to 1.7×10^6 and later stable around 0.92×10^6 for the highest value of the waning rate $\tau_c = 0.9$. It is also evident that the reproduction number moved from an endemic state to a disease-free state in the right panel.

Similar results are obtained in Fig. 9 and the same explanation holds for the dynamics of the influenza population. The influenza dynamics peak in the left panel reduced approximately to 0.36×10^6 and later stable around 0.33×10^6 for the highest value of the waning rate $\omega_i = 0.9$. The influenza dynamics peak in the right panel reduced approximately to 1.4×10^6 and later stable around 0.8×10^6 for the highest value of the waning rate $\tau_i = 0.9$. The result on the right panel is more promising than that of the left panel. The values of R_{inf} decrease with an increase in θ_i and ϵ_i and the disease prevalence in the population decreases as more people get vaccinated. It is also evident that the reproduction number moved from an endemic state to a disease-free state in the right panel.

Fig. 10 shows the dynamics of the co-infection population for the co-infection model (2.15) over time for different values of the COVID-19 effective contact rates (left panel) and different values of co-infection contact rates (right panel). In both panels, $\epsilon_{ci} = \epsilon_i = \epsilon_c = 0.6$, $\theta_i = \theta_{ci} = \theta_c = 0.45$, $\omega_c = \omega_i = \omega_{ci} = \tau_i = \tau_c = \tau_{ci} = 0.85$. Other parameter values are in Table 2. It can be shown on the left panel that an increase in the effective contact rate of COVID-19 will plunge the co-infection population into more problems and the disease will be endemic for a longer period of time. On the right panel, an increase in the effective contact rate for the co-infection dynamics does not produce any notable effects on the co-infection dynamics. This may be a result of our initial assumption that two infections cannot have the same viral load nor can they have the same within-host competitiveness, this means that an infectious co-infected person will transmit the infection that has the highest within-host competitiveness. Here, it is suspected that the COVID-19 transmission rate has a within-host competitive advantage. This is also in tandem with the claim that two viral infections involving SARS-COV-2 do not always go well together in the same cell [70,71].

In Fig. 11, we checked the effects of COVID-19 vaccine-induced immunity waning rate and waning rates for both vaccines on the dynamics of the co-infection model (2.15). The dynamics of the co-infection population over time for different values of the COVID-19 vaccine-induced immunity waning rates is on the left panel while the effect of waning rate for both vaccines is on the right panel. In the left panel, $\epsilon_{ci} = \epsilon_i = \epsilon_c = 0.6$, $\theta_i = \theta_{ci} = \theta_c = 0.45$, $\omega_c = \omega_i = \omega_{ci} = \tau_i = \tau_{ci} = 0.85$. In the right panel, $\epsilon_{ci} = \epsilon_i = \epsilon_c = 0.6$, $\theta_i = \theta_{ci} = \theta_c = 0.45$, $\omega_c = \omega_i = \omega_{ci} = \tau_i = \tau_c = 0.85$. Other parameter values are in Table 2. As in the previous figures such as Figs. 6 and 7, the infected population remains endemic as long as more vaccinated people lose their vaccine-induced immunity waning. Moreover, it can be observed here that the vaccine-induced immunity waning for those that got the two vaccines is more significant than for those who

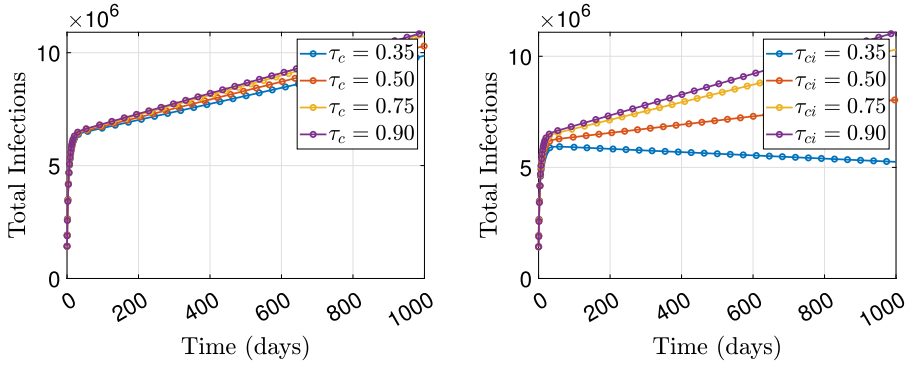

Fig. 11. Effects of the vaccine-induced immunity waning rates on the co-infection dynamics. The dynamics of the co-infection population over time for different values of the COVID-19 vaccine-induced immunity waning rates (left panel) and different values of waning rates for both vaccines (right panel). In the left panel, $\epsilon_{ci} = \epsilon_i = \epsilon_c = 0.6$, $\theta_i = \theta_{ci} = \theta_c = 0.45$, $\omega_c = \omega_i = \omega_{ci} = \tau_i = \tau_{ci} = 0.85$. In the right panel, $\epsilon_{ci} = \epsilon_i = \epsilon_c = 0.6$, $\theta_i = \theta_{ci} = \theta_c = 0.45$, $\omega_c = \omega_i = \omega_{ci} = \tau_i = \tau_c = 0.85$. Other parameter values are in Table 2.

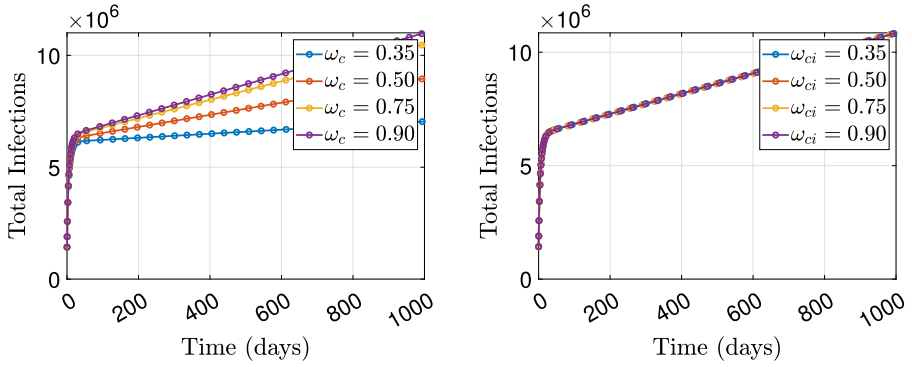

Fig. 12. Effects of the post-recovery immunity waning rates on the co-infection dynamics. The dynamics of the co-infection population over time for different values of the post-recovery immunity waning rates (left panel) and different values of waning rates for both diseases (right panel). In the left panel, $\epsilon_{ci} = \epsilon_i = \epsilon_c = 0.6$, $\theta_i = \theta_{ci} = \theta_c = 0.45$, $\omega_i = \omega_{ci} = \tau_i = \tau_{ci} = 0.85$. In the right panel, $\epsilon_{ci} = \epsilon_i = \epsilon_c = 0.6$, $\theta_i = \theta_{ci} = \theta_c = 0.45$, $\omega_c = \omega_i = \tau_i = \tau_c = 0.85$. Other parameter values are in Table 2.

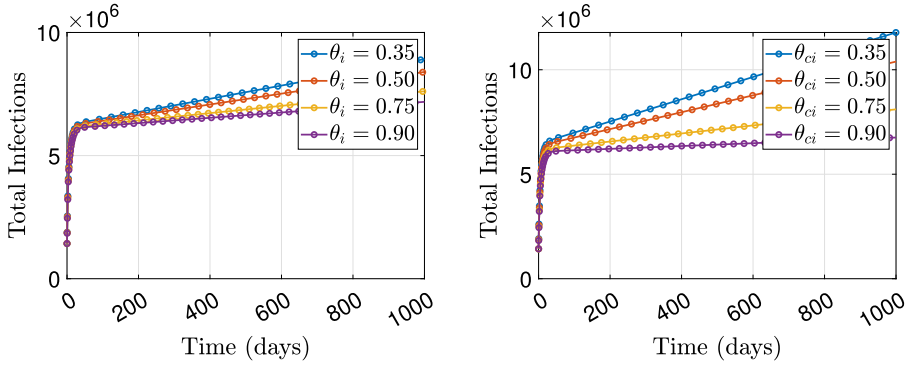

Fig. 13. Effects of the vaccination rates on the co-infection dynamics. The dynamics of the co-infection population over time for different values of the influenza vaccination rates (left panel) and different values of vaccination rate for both diseases (right panel). In the left panel, $\epsilon_{ci} = \epsilon_i = \epsilon_c = 0.6$, $\theta_{ci} = \theta_c = 0.45$, $\omega_i = \omega_{ci} = \tau_i = \tau_c = \tau_{ci} = 0.85$. In the right panel, $\epsilon_{ci} = \epsilon_i = \epsilon_c = 0.6$, $\theta_i = \theta_c = 0.45$, $\omega_c = \omega_i = \tau_i = \tau_c = 0.85$. Other parameter values are in Table 2.

lost their COVID-19 vaccine-induced immunity waning only. A similar explanation can be given for Fig. 12, that is the higher the post-recovery immunity waning, the higher the infection in the community. However, it appears that the COVID-19 post-recovery immunity waning has more effects on the co-infection dynamics than the co-infection post-recovery immunity waning. The previous explanation about the possibility of COVID-19 having a higher competitive advantage may be the reason for this counter-intuitive occurrence. The dynamics of the co-infection population over time for different values of the influenza vaccination rates (left panel) and different values of vaccination rate for both diseases (right panel) is shown in Fig. 13. In the left panel, $\epsilon_{ci} = \epsilon_i = \epsilon_c = 0.6$, $\theta_{ci} = \theta_c = 0.45$, $\omega_i = \omega_{ci} = \tau_i = \tau_c = \tau_{ci} = 0.85$. In the right panel, $\epsilon_{ci} = \epsilon_i = \epsilon_c = 0.6$, $\theta_i = \theta_c = 0.45$, $\omega_c = \omega_i = \tau_i = \tau_c = 0.85$. Other parameter values are in Table 2. In this figure, the effects of vaccination in reducing the spread of infection are evident. The more people get vaccinated, the lower the spread of the disease in the population. It can also be observed that when more people get both COVID-19 and influenza vaccines, the disease will reduce and eventually die out or be kept under control.

6. Conclusion

We developed and analyzed an endemic model for the co-infection dynamics of COVID-19 and the influenza virus using sets of first-order non-linear differential equations. The model incorporates the effects of immunity-waning rates for both diseases. The co-dynamics

population at any time t is represented by $N(t)$. The population is stratified into 12 mutually exclusive populations involving the susceptible $S(t)$, COVID-19 exposed $E_c(t)$, and co-infection exposed population $E_{ci}(t)$. The vaccinated individuals against COVID-19, influenza, and both diseases are respectively denoted by $V_c(t), V_i(t)$ and $V_{ci}(t)$. The COVID-19, influenza and co-infected individuals respectively denoted by $I_c(t), I_i(t)$ and I_{ci} become recovered and move to the compartments $R_c(t), R_i(t)$ and $R_{ci}(t)$ respectively. A fraction of the population loses their immunity-waning rates a few days after getting vaccinated.

After establishing the boundedness and positivity of the solution through some Theorems and Lemmas, the disease-free and endemic equilibria for both COVID-19 and influenza virus were presented. This was followed by the calculation of the reproduction number for both diseases as well as the co-dynamics model. The local asymptotic stability of both the disease-free and endemic equilibria was presented using some theorems, although, the detailed proofs were ignored for being elementary calculations. It was observed from the results that when the reproduction number is less than unity, the infected populations diminish steadily toward zero within the early period of the infection while the uninfected populations increase steadily and later stabilize at the top. The recovered population decreases steadily as expected. This means that whenever the COVID-19/influenza reproduction number becomes less than 1, the disease dies out, and both the susceptible and vaccinated populations become stable. It also means that if the average number of new COVID-19/influenza infections generated by a single infection introduced into a susceptible population in any province in Israel is less than 1, then the virus will be eliminated in the population. On the other hand, if the COVID-19/influenza reproduction number is greater than unity, the virus becomes endemic for the foreseeable future.

In the numerical simulation section, the demography of Israel was used. We explained how the initial conditions were extracted and calculated as appeared in Table 3. How the parameter values were deduced, assumed, or calculated was also discussed and properly referenced in Table 2. The effects of some key parameters of both the sub-model and the co-infection models were properly investigated. We make use of the ode45 package in MATLAB R2022b for the simulation. The COVID-19 epidemic peak was at the highest level for the highest value of the post-recovery immunity waning rate $\omega_c = 0.9$. A similar result was obtained for the effects of the vaccine-induced immunity waning rate whose increase increases the COVID-19 reproduction number. It was also observed that the post-recovery waning rate has lesser effects on the disease dynamics compared to the vaccine-induced immunity waning rate. One of the reasons for this observation is that the COVID-19 reproduction number R_{cov} does not depend on the parameter ω_c because the value of R_{cov} remains constant for all values of ω_c thereby showing lesser effects on the COVID-19 dynamics. Similar results were obtained in the numerical simulation of the effects of immunity waning on the influenza dynamics.

We further investigated the dynamics of the COVID-19 and influenza populations over time under vaccination strategies with varying vaccine efficacy rates. The COVID-19 epidemic peak reduced drastically when the vaccination and vaccine efficacy rates are at the highest level. For this scenario, the reproduction numbers also changed from an endemic state to a disease-free state as the vaccination rate increased. This shows that the vaccination and vaccine efficacy rates have significant effects on the disease dynamics as the reproduction number reduced drastically from its previous value. Although the reproduction numbers were still greater than unity in some cases because they are independent of the post-recovery immunity waning rates.

Next, we showed the dynamics of the co-infection population over time for different values of the COVID-19 effective contact rates and different values of co-infection contact rates. It was discovered that an increase in the effective contact rate of COVID-19 will plunge the co-infection population into more problems and the disease will be endemic for a longer period of time. More so, an increase in the effective contact rate for the co-infection dynamics does not produce any notable effects on the co-infection dynamics. This may be, is as a result of our initial assumption that two infections cannot have the same viral load nor can they have the same within-host competitiveness, this means that an infectious co-infected person will transmit the infection that has the highest within-host competitiveness. Here, it is suspected that the COVID-19 transmission rate has a within-host competitive advantage over influenza. This is also in tandem with the claim that two viral infections involving SARS-COV-2 do not always go well together in the same cell [70].

Next, we further checked the effects of the COVID-19 vaccine-induced immunity waning rate and the waning rates for both vaccines on the dynamics of the co-infection model. We observed that the infected population remains endemic as long as more vaccinated people lose their vaccine-induced immunity waning. Moreover, it was also observed here that the vaccine-induced immunity waning of those that got the two vaccines has more significant impact on diseases dynamics than those who lost their COVID-19 vaccine-induced immunity waning only. However, it appears that the COVID-19 post-recovery immunity waning has more effects on the co-infection dynamics than the co-infection post-recovery immunity waning rate. The previous explanation about the possibility of COVID-19 having a higher competitive advantage may be the reason for this counter-intuitive occurrence.

Lastly, we investigated the dynamics of the co-infection population over time for different values of the influenza vaccination rates and different values of vaccination rates for both diseases. It was observed that the effects of vaccination in reducing the spread of infection are evident and more pronounced in the co-infection population than that in the influenza population who only got the influenza vaccine. The more people get vaccinated, the lower the spread of the disease in the population. It can also be observed that when more people get both COVID-19 and influenza vaccines, the disease will reduce more and eventually die out in a short while. The findings of this study will also assist the government and Non-Governmental Organisations (NGOs) to come up with policies and programs formulations vaccination policies on disease control to achieve an optimum result

An interesting and important future study would involve fitting the sub-model or the co-infection model to the reported case of COVID-19 and influenza in Israel where the estimated parameters would then be used to study the severity of COVID-19 and influenza in different cities. Another future direction would be to stratify the COVID and influenza sub-model into different age groups such that they interact with each other. This would make it easy to study the contribution of each age group to the disease dynamics.

Declaration of competing interest

None

Data availability

No data was used for the research described in the article.

Funding statement

No funding was received for this work

References

[1] WHO dashboard, WHO Coronavirus (COVID-19) Dashboard, World Health Organization (WHO), https://covid19.who.int/, accessed April 17, 2022.
[2] WHO's COVID-19 Response Timeline, World Health Organization (WHO), https://www.who.int/emergencies/diseases/novel-coronavirus-2019/interactive-timeline/#category-Information, (accessed Nov 21, 2022).

[3] https://www.worldometers.info/coronavirus/ (Accessed on Nov 21, 2022).
[4] Available from: https://www.who.int/emergencies/diseases/novel-coronavirus-2019 (Accessed on Nov 21, 2022).
[5] R.C. Khanna, M.V. Cicinelli, S.S. Gilbert, S.G. Honavar, G.V. Murthy, COVID-19 pandemic: Lessons learned and future directions, Indian J. Ophthalmol. 68 (5) (2020) 703.
[6] S.W.X. Ong, Y.K. Tan, P.Y. Chia, T.H. Lee, O.T. Ng, M.S.Y. Wong, K. Marimuthu, Air, surface environmental, and personal protective equipment contamination by severe acute respiratory syndrome coronavirus 2 (SARS-CoV-2) from a symptomatic patient, JAMA 323 (16) (2020) 1610–1612.
[7] R. Karia, I. Gupta, H. Khandait, A. Yadav, A. Yadav, COVID-19 and its modes of transmission, SN Compr. Clin. Med. 2 (10) (2020) 1798–1801.
[8] M.O. Adeniyi, S.I. Oke, M.I. Ekum, T. Benson, M.O. Adewole, Assessing the impact of public compliance on the use of non-pharmaceutical intervention with cost-effectiveness analysis on the transmission dynamics of COVID-19: Insight from mathematical modeling, in: Modeling, Control and Drug Development for COVID-19 Outbreak Prevention, Springer, Cham, 2022, pp. 579–618.
[9] S. Ullah, M.A. Khan, Modeling the impact of non-pharmaceutical interventions on the dynamics of novel coronavirus with optimal control analysis with a case study, Chaos, Solitons Fract. lem 139 (2020) 110075.
[10] L. Lemecha Obsu, S. Feyissa Balcha, Optimal control strategies for the transmission risk of COVID-19, J. Biol. Dyn. 14 (1) (2020) 590–607.
[11] Z.H. Shen, Y.M. Chu, M.A. Khan, S. Muhammad, O.A. Al-Hartomy, M. Higazy, Mathematical modeling and optimal control of the COVID-19 dynamics, Results Phys. 31 (2021) 105028.
[12] J. Chen, R. Wang, N.B. Gilby, G.W. Wei, Omicron variant (b. 1.1. 529): infectivity, vaccine breakthrough, and antibody resistance, J. Chem. Inf. Model. 62 (2) (2022) 412–422.
[13] P. Mlcochova, S. Kemp, M.S. Dhar, G. Papa, B. Meng, S. Mishra, Ravindra K. ...Gupta1, SARS-CoV-2 b. 1.617. 2 delta variant emergence and vaccine breakthrough, 2021.
[14] M. Derouich, A. Boutayeb, An avian influenza mathematical model, Appl. Math. Sci. 2 (36) (2008) 1749–1760.
[15] Seasonal influenza, 2022, Available on https://www.who.int/health-topics/influenza-seasonal#tab=tab_1. Accessed on November 21, 2022.
[16] T. Smieszek, G. Lazzari, M. Salathé, Assessing the dynamics and control of droplet-and aerosol-transmitted influenza using an indoor positioning system, Sci. Rep. 9 (1) (2019) 1–10.
[17] M.M. Ojo, T.O. Benson, O.J. Peter, E.F.D. Goufo, Nonlinear optimal control strategies for a mathematical model of COVID-19 and influenza co-infection, Physica A 607 (2022) 128173.
[18] L. Bai, Y. Zhao, J. Dong, S. Liang, M. Guo, X. Liu, X. Wang, Z. Huang, X. Sun, Z. Zhang, et al., Coinfection with influenza a virus enhances SARS-CoV-2 infectivity, Cell. Res. 31 (2021) 395–403.
[19] X. Xiang, Z.H. Wang, L.L. Ye, X.L. He, X.S. Wei, Y.L. Ma, H. Li, L. Chen, X.R. Wang, Q. Zhou, Co-infection of SARS-COV-2 and influenza a virus: A case series and fast review, Curr. Med. Sci. 41 (2021) 51–57.
[20] O.J. Peter, H.S. Panigoro, A. Abidemi, M.M. Ojo, F.A. Oguntolu, Mathematical model of COVID-19 pandemic with double dose vaccination, Acta Biotheor. 71 (2) (2023) 9.
[21] B. Kammegne, K. Oshinubi, O. Babasola, O.J. Peter, O.B. Longe, R.B. Ogunrinde, J. .Demongeot, Mathematical modelling of the spatial distribution of a COVID-19 outbreak with vaccination using diffusion equation, Pathogens 12 (1) (2023) 88.
[22] M.M. Ojo, O.J. Peter, E.F.D. Goufo, K.S. Nisar, A mathematical model for the co-dynamics of COVID-19 and tuberculosis, Math. Comput. Simulation (2023).
[23] K. Oshinubi, A. Amakor, O.J. Peter, M. Rachdi, J. Demongeot, Approach to COVID-19 time series data using deep learning and spectral analysis methods, Aims Bioeng. 9 (2022) 1–21.
[24] O. Babasola, O. Kayode, O.J. Peter, F.C. Onwuegbuche, F.A. Oguntolu, Time-delayed modelling of the covid-19 dynamics with a convex incidence rate, Inform. Med. Unlocked (2022) 101124.
[25] A.A. Ayoade, P.A. Ikpechukwu, S. Thota, O.J. Peter, Modeling the effect of quarantine and hospitalization on the spread of COVID-19 during the toughest period of the pandemic, J. Mahani Math. Res. (2022) 339–361.
[26] O.J. Peter, S. Qureshi, A. Yusuf, M. Al-Shomrani, A.A. Idowu, A new mathematical model of COVID-19 using real data from Pakistan, Results Phys. 24 (2021) 104098.
[27] A.I. Abioye, O.J. Peter, H.A. Ogunseye, F.A. Oguntolu, K. Oshinubi, A.A. Ibrahim, I. Khan, Mathematical model of COVID-19 in Nigeria with optimal control, Results Phys. 28 (2021) 104598.
[28] O.J. Peter, A.S. Shaikh, M.O. Ibrahim, K.S. Nisar, D. Baleanu, I. Khan, A.I. Abioye, Analysis and dynamics of fractional order mathematical model of COVID-19 in Nigeria using atangana-baleanu operator, 2021.
[29] A.I. Abioye, M.D. Umoh, O.J. Peter, H.O. Edogbanya, F.A. Oguntolu, O. Kayode, S. Amadiegwu, Forecasting of COVID-19 pandemic in Nigeria using real statistical data, Commun. Math. Biol. Neurosci. (2021) Article-ID.
[30] A. Awasthi, A mathematical model for transmission dynamics of COVID-19 infection, Eur. Phys. J. Plus 138 (3) (2023) 285.
[31] A. Yousef, F. Bozkurt, T. Abdeljawad, E. Emreizeeq, A mathematical model of COVID-19 and the multi fears of the community during the epidemiological stage, J. Comput. Appl. Math. 419 (2023) 114624.
[32] B. Maayah, O.A. Arqub, S. Alnabulsi, H. Alsulami, Numerical solutions and geometric attractors of a fractional model of the cancer-immune based on the Atangana-Baleanu-Caputo derivative and the reproducing kernel scheme, Chinese J. Phys. 80 (2022) 463–483.
[33] J. Paget, S. Caini, B. Cowling, S. Esposito, A.R. Falsey, A. Gentile, J. Kyncl, C. MacIntyre, R. Pitman, B. Lina, The impact of influenza vaccination on the COVID-19 pandemic? Evidence and lessons for public health policies, Vaccine 38 (2020) 6485–6486.
[34] D. Thindwa, M. Garcia Quesada, Y. Liu, J. Bennett, C. Cohen, M.D. Knoll, A. von Gottberg, K. Hayford, S. Flasche, Use of seasonal influenza and pneumococcal polysaccharide vaccines in older adults to reduce COVID-19 mortality, Vaccine 38 (2020) 5398–5401, [Google Scholar] [CrossRef] [PubMed].
[35] Y. Goldberg, M. Mandel, Y.M. Bar-On, O. Bodenheimer, L. Freedman, E.J. Haas, A. .Huppert, Waning immunity after the BNT162b2 vaccine in Israel, New Engl. J. Med. 385 (24) (2021) e85.
[36] E. Dolgin, COVID vaccine immunity is waning-how much does that matter, Nature 597 (7878) (2021) 606–607.
[37] S. Bhowmick, I.M. Sokolov, H.H. Lentz, Decoding the double trouble: A mathematical modelling of co-infection dynamics of SARS-CoV-2 and influenza-like illness, 2022, arXiv preprint arXiv:2210.05649.
[38] R. Ozaras, R. Cirpin, A. Duran, H. Duman, O. Arslan, Y. Bakcan, S. .Bilir, Influenza and COVID-19 coinfection: report of six cases and review of the literature, J. Med. Virol. 92 (11) (2020) 2657–2665.
[39] V.M. Konala, S. Adapa, S. Naramala, A. Chenna, S. Lamichhane, P.R. Garlapati, V. .Gayam, A case series of patients coinfected with influenza and COVID-19, J. Invest. Med. High Impact Case Rep. 8 (2020) 2324709620934674.
[40] Q. Ding, P. Lu, Y. Fan, Y. Xia, M. Liu, The clinical characteristics of pneumonia patients coinfected with 2019 novel coronavirus and influenza virus in wuhan, Chin. J. Med. Virol. 92 (9) (2020) 1549–1555.
[41] M. Dadashi, S. Khaleghnejad, P.Abedi. Elkhichi, M. Goudarzi, H. Goudarzi, A. Taghavi, B... Hajikhani, COVID-19 and influenza co-infection: a systematic review and meta-analysis, Front. Med. 8 (971) (2021).
[42] C. Janssen, A. Mosnier, G. Gavazzi, B. Combadière, P. Crepey, J. Gaillat, E. .Botelho-Nevers, Coadministration of seasonal influenza and COVID-19 vaccines: A systematic review of clinical studies, Hum. Vaccines Immunother. (2022) 2131166.
[43] C.D.C. Covid, V.B.C.I. Team, M. Birhane, S. Bressler, G. Chang, T. Clark, A. .Trujillo, COVID-19 vaccine breakthrough infections reported to CDC—United States, january 1–april 30, 2021, Morb. Mortal. Wkly. Rep. 70 (21) (2021) 792.
[44] S. Anjan, Y. Natori, A.A.F. Betances, M.S. Agritelley, A. Mattiazzi, L. Arosemena, L.M. .Abbo, Breakthrough COVID-19 infections after mRNA vaccination in solid organ transplant recipients in miami, florida, Transplantation 105 (10) (2021) e139.
[45] J. Sun, Q. Zheng, V. Madhira, A.L. Olex, A.J. Anzalone, A. Vinson, E.A. .Chirischilles, Association between immune dysfunction and COVID-19 breakthrough infection after SARS-CoV-2 vaccination in the US, JAMA Int. Med. 182 (2) (2022) 153–162.
[46] M.A. Zoran, R.S. Savastru, D.M. Savastru, M.N. Tautan, Assessing the relationship between surface levels of PM2.5 and PM10 particulate matter impact on COVID-19 in milan, Italy, Sci. Total Environ. 738 (2020) 139825, http://dx.doi.org/10.1016/j.scitotenv.2020.139825.
[47] E.A. Iboi, C.N. Ngonghala, A.B. Gumel, Will an imperfect vaccine curtail the COVID-19 pandemic in the US? Infect. Dis. Modell. 5 (2020) 510–524.
[48] F. Haghpanah, G. Lin, S.A. Levin, E. Klein, Analysis of the potential impact of durability, timing, and transmission blocking of COVID-19 vaccine on morbidity and mortality, EClinicalMedicine 35 (2021) 100863.
[49] M. Rabiu, S.A. Iyaniwura, Assessing the potential impact of immunity waning on the dynamics of COVID-19 in South Africa: an endemic model of COVID-19, Nonlinear Dynam. (2022) 1–21.
[50] Total immigration to Israel by year, 1948-present, 2022, https://www.jewishvirtuallibrary.org/total-immigration-to-israel-by-year. Accessed on 29/12/2022.
[51] Israel birth rate 1950–2022, 2022, Available on https://www.macrotrends.net/countries/ISR/israel/birth-rate. Accessed on 29/12/2022.
[52] A.B. Gumel, E.A. Iboi, C.N. Ngonghala, G.A. Ngwa, Mathematical assessment of the roles of vaccination and non-pharmaceutical interventions on COVID-19 dynamics: a multigroup modeling approach, 2020.
[53] Z. Jin, J. Zhang, L.P. Song, G.Q. Sun, J. Kan, H. Zhu, Modelling and analysis of influenza a (h1n1) on networks, BMC Public Health 11 (1) (2011) 1–9.
[54] M. Rabiu, S.A. Iyaniwura, Assessing the potential impact of immunity waning on the dynamics of COVID-19 in South Africa: an endemic model of COVID-19, Nonlinear Dyn. 109 (2022) 203–223, http://dx.doi.org/10.1007/s11071-022-07225-9.
[55] Z. Zhao, X. Li, F. Liu, G. Zhu, C. Ma, L. Wang, Prediction of the COVID-19 spread in african countries and implications for prevention and control: A case study in South Africa, Egypt, Algeria, Nigeria, Senegal and Kenya, Sci. Total Environ. 729 (2020) 138959.
[56] C.W. Kanyiri, K. Mark, L. Luboobi, Mathematical analysis of influenza a dynamics in the emergence of drug resistance, Comput. Math. Methods Med. 2018 (2018).

[57] T. Ganyani, C. Kremer, D. Chen, A. Torneri, C. Faes, J. Wallinga, N. Hens, Estimating the generation interval for coronavirus disease (COVID-19) based on symptom onset data 2020, Eurosurveillance 25 (17) (2020) 2000257.
[58] un Li, Xuhua Guan, Peng Wu, Xiaoye Wang, Lei Zhou, Yeqing Tong, Ruiqi Ren, Kathy S.M. Leung, Eric H.Y. Lau, Jessica Y. Wong, et al., Early transmission dynamics in wuhan, china, of novel coronavirus infected pneumonia, New Engl. J. Med. (2020).
[59] The world population review, 2022, Available on https://worldpopulationreview.com/countries/israel-population, Accessed on 28/12/2022.
[60] L.C. Tindale, M. Coombe, J.E. Stockdale, E.S. Garlock, W.Y.V. Lau, M. Saraswat, C. .Colijn, Transmission interval estimates suggest pre-symptomatic spread of COVID-19, 2020, MedRxiv.
[61] O. Diekmann, J.A.P. Heesterbeek, J.A. Metz, On the definition and the computation of the basic reproduction ratio r 0 in models for infectious diseases in heterogeneous populations, J. Math. Biol. 28 (4) (1990) 365–382.
[62] P. Van den Driessche, J. Watmough, Reproduction numbers and sub-threshold endemic equilibria for compartmental models of disease transmission, Math. Biosci. 180 (1–2) (2002) 29–48.
[63] P. Van den Driessche, J. Watmough, Reproduction numbers and sub-threshold endemic equilibria for compartmental models of disease transmission, Math. Biosci. 180 (1–2) (2002) 29–48.
[64] M.A. Safi, A.B. Gumel, Mathematical analysis of a disease transmission model with quarantine, isolation and an imperfect vaccine, Comput. Math. Appl. 61 (10) (2011) 3044–3070.
[65] S.M. Garba, M.A. Safi, S. Usaini, Mathematical model for assessing the impact of vaccination and treatment on measles transmission dynamics, Math. Methods Appl. Sci. 40 (18) (2017) 6371–6388.
[66] Covid-19 coronavirus pandemic, 2022, https://www.worldometers.info/coronavirus/#countries, accessed on 28/12/2022.
[67] E.J. Haas, F.J. Angulo, J.M. McLaughlin, E. Anis, S.R. Singer, F. Khan, S. .Alroy-Preis, Impact and effectiveness of mRNA BNT162b2 vaccine against SARS-CoV-2 infections and COVID-19 cases, hospitalizations, and deaths following a nationwide vaccination campaign in Israel: an observational study using national surveillance data, Lancet 397 (10287) (2021) 1819–1829.
[68] Surveillance of influenze-like illness in Israel, weekly update, 2022, https://www.health.gov.il/English/MinistryUnits/ICDC/Infectious_diseases/Flu/Pages/FWR.aspx. Accessed on 29/12/2022.
[69] 'Flurona': Israel records its first case of patient with COVID and flu at same time. https://www.timesofisrael.com/flurona-israel-records-its-first-case-of-patient-with-covid-and-flu-at-same-time/.
[70] Competition between respiratory viruses may hold off a 'tripledemic' this winter, 2022, https://www.science.org/content/article/competition-between-respiratory-viruses-may-hold-tripledemic-winter. Accessed on 20, 2022.
[71] B. Maayah, A. Moussaoui, S. Bushnaq, O. Abu Arqub, The multistep Laplace optimized decomposition method for solving fractional-order coronavirus disease model (COVID-19) via the Caputo fractional approach, Demonstratio Math. 55 (1) (2022) 963–977.